Enhanced Production of BTX from PET-LDPE Co-Pyrolysis via Ga- and Zn-Impregnated HZSM-5 Catalysts

Oğuzhan Akin, Qing He, Mohammadhossein Havaei, Fatma Defne Calik, Daniël Withoeck , Robin John Varghese, Parviz Yazdani, Paul Van Steenberge, Kevin M. Van Geem[*]

Laboratory for Chemical Technology (LCT), Department of Materials, Textiles and Chemical Engineering, Faculty of Engineering & Architecture, Ghent University, Technologiepark-Zwijnaarde 125, 9052 Zwijnaarde, Belgium

[*]Corresponding author: Kevin.VanGeem@UGent.be

Key Words: Plastics, catalysts, chemical recycling, pyrolysis, olefins

ABSTRACT

The coexistence of polyethylene terephthalate (PET) and polyolefins in plastic waste poses a significant challenge for pyrolysis-based recycling, as PET decomposition generates oxygenates that reduce product quality. To address this, we developed a two-stage reactor system that catalytically upgrades vapors from PET–LDPE mixtures using Ga- and Zn-impregnated HZSM-5 catalysts. XPS analysis revealed that impregnation with Ga and Zn leads to the formation of GaO_x and $ZnOH^+$ species, which introduce new Lewis acid sites. When these sites are located near Brønsted acid sites, synergistic interactions enhance both deoxygenation and aromatization, improving the catalytic performance of HZSM-5. At 600 °C, PET pyrolysis produces significant amounts of CO_2, CO, and benzoic acid, resulting in oxygen-rich pyrolysis oil. While unmodified HZSM-5 achieves full deoxygenation, the resulting PyOil yield is modest, ranging from 24 to 34 wt.%. In contrast, Ga- and Zn-modified catalysts increase PyOil yield to ~50 wt.% and improve mono-aromatic (BTX) selectivity to 80–89% by shifting the acid site distribution toward weaker acidity, thereby favoring decarboxylation, decarbonylation, and aromatization. Notably, Zn-HZSM-5 maintained high BTX selectivity even with increasing PET content, outperforming Ga-HZSM-5, which exhibited higher polyaromatic hydrocarbon formation under similar conditions. These results demonstrate the potential of Ga- and Zn-modified HZSM-5 catalysts for the efficient conversion of mixed plastic waste into BTX-rich oils suitable for fuel and chemical applications.

1 Introduction

Plastics play a vital role in modern society, with applications that extend across various sectors, including packaging, construction, textiles, automotive, electronics, and medicine. Despite their widespread use, the burgeoning demand for plastics, combined with suboptimal waste management practices, has led to significant accumulation of plastic waste. In response, substantial research efforts have been dedicated to advancing the efficacy of plastic recycling technologies [1, 2].

Pyrolysis thermally breaks the chemical bonds of polymers in an inert atmosphere, potentially generating valuable chemicals. It has been extensively studied for polyolefins, the largest proportion of municipal solid waste. Polyolefins, when pyrolyzed, produce gasoline and diesel-range hydrocarbons. Catalytic pyrolysis of polyolefins enables tuning the product distribution toward valuable light olefins (i.e., ethylene, propylene, butenes) and aromatics. Our previous studies have demonstrated that HZSM-5 is an effective catalyst for producing light olefins via polyolefin pyrolysis [3-7]. Moreover, modifying HZSM-5 with mesopore introduction and phosphorus impregnation enhances the selectivity to light olefins and improves catalyst stability [5, 7, 8]. However, these studies primarily focused on the cracking of virgin polyolefins or polyolefins with limited contaminants (8 wt.% non-polyolefins, with only 1 wt.% PET) and reported insignificant changes in the product distribution caused by the contaminants [3, 4].

Polyethylene terephthalate (PET) is the third most widely used plastic resin, accounting for ~ 6 wt.% of global plastic production [9]. Despite its widespread use, the pyrolysis of PET has received considerably less attention compared to polyolefins [2]. One reason for this is that well-sorted PET bottles can be efficiently recycled through mechanical processes without the issue of downcycling, which requires less energy and complexity than chemical recycling methods such as pyrolysis or catalytic cracking [10]. However, PET applications extend beyond

bottles; it is frequently combined with other resins and materials to produce fibers, sheets, and films. For example, multilayer packaging often blends PET with polyolefins, which requires advanced delamination processes for recycling and contributes to lower overall recycling rates for PET [11-13].

PET pyrolysis yields benzoic acid, terephthalic acid (TPA), and various oxygenated aromatics that are corrosive, prone to causing pipe blockages, and incompatible with conventional fuel specifications [14-17]. Catalytic upgrading of PET pyrolysis vapors could help mitigate this issue, as these oxygenates can be catalytically converted into aromatics. Artetxe et al. reported that benzoic acid, after CO and CO_2, is the primary product of PET pyrolysis at the temperature range of 500-600 °C [18]. They observed that increasing the temperature from 500 °C to 600 °C decreased the benzoic acid yield by 10 wt.% but only improved the yield of other oxygenates, showing the need for catalytic conversion of these acids into aromatics. For instance, the research group of Yoshioka has reported the use of calcium oxide (CaO) as a catalyst to suppress organic acid production in favor of benzene formation [19-21], revealing that the basic strength of the catalyst significantly improves aromatic hydrocarbon formation [22].

Further research has explored the catalytic co-pyrolysis of PET and polyolefins. Okonsky et al. investigated the co-pyrolysis of low-density polyethylene (LDPE) and PET using catalysts such as HZSM-5, HY, and H-beta, reporting low yields of benzoic acid (<1%) alongside high aromatic yields, showing similarities in the behavior of basic and acidic catalysts [13]. Du et al. investigated the catalytic fast pyrolysis of PET-rich carpet waste using HZSM-5 and CaO as catalysts [14]. Their study demonstrated that both catalysts were highly effective in removing carboxyl groups from acids and promoting the formation of aromatics. Notably, CaO exhibited a higher selectivity toward benzene production, while HZSM-5 also facilitated the formation

of other aromatics, including indene and naphthalene. This difference in product distribution is attributed to the distinct catalytic mechanisms of HZSM-5 and CaO. The hydrocarbon pool mechanism in HZSM-5 was originally proposed for methanol-to-olefins (MTO) reactions, wherein methanol diffuses into the zeolite pores and forms $(CH_2)_n$ adsorbate, which continuously generate olefins and aromatics through a cyclic reaction network. More recently, this mechanism has also been proposed for plastic and biomass pyrolysis [23], where it is reported to facilitate alkylation and hydrogen transfer reactions, ultimately promoting the formation of monoaromatics and polyaromatics [14, 24, 25]. Meanwhile, CaO is known for primarily catalyzing decarboxylation reactions, converting terephthalic acid into benzene and CO_2 [20, 26].

There are several catalyst modification strategies to optimize product distribution in catalytic pyrolysis, with metal oxide impregnation on zeolites being one of the most effective approaches for tailoring catalysts to meet specific product requirements for various pyrolysis feedstocks. For example, impregnation of HZSM-5 with Ga or Zn has been shown to increase the density of Lewis acid sites on the catalyst surface [27, 28]. These newly introduced Lewis acid sites catalyze the dehydrogenation of olefins to the corresponding dienes and aromatics, while adjacent Brønsted sites drive the subsequent cyclization and hydride-transfer steps that complete the BTX pathway. When Lewis acid sites are in close proximity to Brønsted acid sites, this synergistic environment can accelerate overall aromatization [29]. Consistent with this mechanism, several studies have reported that such modifications promote aromatic hydrocarbon formation during the catalytic pyrolysis of polyolefins, including polyethylene and polypropylene [28, 30-33]. Typical plastic pyrolysis studies are predominantly conducted with polyolefins, which lack oxygenated compounds, making it challenging to investigate the effects of Ga and Zn modification on deoxygenation reactions in such systems. However, several studies on biomass pyrolysis provide valuable insights into the deoxygenation capabilities of

prompted zeolites. For example, both Ga and Zn modifications are reported to be highly effective for the aromatization and deoxygenation of biomass-derived pyrolysis products [34-37]. Uslamin et al. demonstrated that Ga incorporation into HZSM-5 replaces Brønsted acid sites with Lewis acid sites, significantly improving aromatic selectivity in catalytic furan conversion [35]. Similarly, Tamiyakul et al. investigated the impact of Ga and Zn impregnation on HZSM-5 for converting palm fatty acid distillate to aromatics, observing increased aromatic selectivity for both modifications [34]. Interestingly, Zn impregnation was found to produce higher aromatic yields than Ga-HZSM-5. This enhancement was attributed to the formation of two zinc species: Zn^{2+}, which promotes dehydrogenation reactions critical for aromatic formation, and ZnO, which facilitates decarboxylation of oxygenates, leading to CO_x generation [34]. Qian et al. further confirmed that Zn^{2+} is the active species for aromatic formation during HDPE pyrolysis over Zn-modified HZSM-5, while ZnO remains inert in the absence of oxygenates [28]. For Ga-modified HZSM-5, Lai et al. proposed two distinct active sites that operate via separate pathways during methanol conversion: surface Ga cations enhance propylene aromatization through dehydrogenation, while bifunctional Ga^{+} species also catalyze benzene alkylation with ethylene [38].

Given that PET and polyolefins are often co-present in plastic waste and PET pyrolysis features significant quantities of oxygenates, it is of particular interest to investigate the catalytic upgrading of LDPE and PET co-pyrolysis vapors to produce high-value products such as light olefins and benzene-toluene-ethylbenzene-xylene (BTX). Although the separate and mixed thermal pyrolysis of LDPE and PET have been extensively studied [39-43], the catalytic co-pyrolysis of these polymers, particularly involving vapor-phase upgrading in a two-stage reactor system, remains underexplored. Furthermore, most previous catalytic studies have primarily focused on in situ configurations, where the catalyst is directly mixed with the feedstock [13, 40, 44-48].

In our previous studies, we demonstrated that both parent HZSM-5 and phosphorus-modified HZSM-5 are highly effective for converting polyolefins into light olefins (C_2–C_4), resulting in high PyGas and low PyOil yields. While this is beneficial for achieving circularity in polyolefin recycling, it becomes less favorable in the context of PET-LDPE co-pyrolysis. This is because PET, being oxygen-rich, generates intermediates that inherently favor the formation of aromatics and non-condensable gases (CO, CO_2), even in the presence of unmodified HZSM-5. Simultaneously, the zeolite continues to convert LDPE-derived hydrocarbons predominantly into light olefins, sustaining a high PyGas output. In such mixed-feed systems, the gaseous product stream contains a mixture of olefins, CO and CO_2, complicating downstream separation and negatively impacting overall process efficiency. Hence, Ga- and Zn-modified HZSM-5 catalysts offer a strategic advantage by promoting aromatization not only of PET-derived oxygenates but also of LDPE-derived hydrocarbons. These metal promoters facilitate hydrogen transfer and dehydrocyclization reactions, thereby enhancing BTX selectivity and increasing both the yield and quality of the PyOil fraction. The primary objectives of this study are to maximize the yields BTX and evaluate potential synergistic effects between the LDPE and PET pyrolysis vapors during catalytic cracking. Hence, the catalytic upgrading of pyrolysis vapors of PET, LDPE, and PET-LDPE mixtures with varying PET to LDPE ratios (3:1, 1:1, and 1:3) were investigated using the micro-pyrolyzer facility combined with comprehensive two-dimensional gas chromatography (GCxGC-FID/TOF-MS) and a separate customized multicolumn GC (Trace 1310) for the analysis of light gases. This analytical approach enables accurate identification and quantification of plastic waste-derived mixtures, shedding light on the intricate process of pyrolysis and catalyst performance.

2 Experimental

2.1 Materials

Polyethylene terephthalate (PET) and benzoic acid (≥99.5% purity) were purchased from Sigma-Aldrich. Virgin low-density polyethylene (LDPE) resin (grade LD150AC) was obtained from ExxonMobil. The number-average molar masses of PET and LDPE were determined to be 7,894 g/mol and 126,329 g/mol, respectively, using size exclusion chromatography (SEC). Detailed information on the SEC methodology is provided in the Supplementary Information. The elemental composition of PET was previously determined to be 62.0 wt.% C, 4.4 wt.% H, with the remainder attributed to oxygen [49]. For LDPE, the elemental composition was 85.0 wt.% C and 15.0 wt.% H, as reported in our previous study [4].

PET was received as granules and LDPE as pellets; both materials were pulverized using a cutting mill and subsequently further ground in a cryogenic mill. The ground samples were sieved to a particle size of ≤ 300 µm to minimize heat and mass transfer limitations during pyrolysis.

The ZSM-5 zeolite (CBV5524G) with a Si/Al ratio of 25 was purchased from Zeolyst International. Gallium nitrate hydrate ($Ga(NO_3)_3 \cdot xH2O$, 99.9% purity) and zinc nitrate hexahydrate ($Zn(NO_3)_2 \cdot 6H_2O$, 99.0 wt.%) were obtained from Sigma-Aldrich.

2.2 Catalyst Synthesis

The parent ZSM-5 zeolite (CBV5524G) was first calcined at 550 °C for 6 hours to obtain the protonated form, HZSM-5. Metal-supported catalysts were then prepared by wet impregnation with a loading of 1 wt.%, using a solution volume based on the saturated water adsorption capacity of the zeolite [50]. The impregnated samples were dried overnight at 120 °C and calcined at 550 °C for 6 hours. The resulting promoted zeolites were designated as Ga-HZSM-5 and Zn-HZSM-5. Subsequently, these catalysts were pelletized, ground, and sieved to a

particle size of 100–300 μm. Finally, the catalysts were stored in sealed vials within a desiccator until reactor loading. Before the catalytic reaction, the loaded catalysts were pretreated in the reactor at 600 °C under a continuous helium flow for 15 minutes to remove any adsorbed moisture.

2.3 Catalyst characterization

2.3.1 Temperature-programmed desorption of NH_3

The acidity of the catalyst was investigated by using ammonia temperature-programmed desorption (NH_3-TPD, Micrometrics Autochem II). For each test, ~0.1 g of catalyst was loaded into a U-shaped quartz reactor. The sample was pretreated by heating to 550 °C under He atmosphere and held for 30 minutes, followed by cooling to 100 °C. The flow was then switched to NH_3 (4% NH_3 in He), and the sample was exposed to allow the adsorption of NH_3 on the acidic sites of the catalyst for 30 minutes. Subsequently, the flow was switched back to He and maintained at 100°C for 120 minutes to remove physically adsorbed NH_3. Finally, temperature-programmed desorption was initiated at a heating rate of 10 °C/min to 600 °C, and the desorbed NH_3 was measured using a thermal conductivity detector (TCD).

2.3.2 Surface morphology and elemental analysis

Scanning electron microscopy coupled with energy-dispersive X-ray spectroscopy (SEM-EDX, JSM-5400, INCAx) was used to analyze the catalyst particle morphology and surface elemental distribution. The test voltage was set to 20 kV. Five particles were randomly selected for elemental analysis for each sample, and the results were averaged.

2.3.3 X-ray photoelectron spectroscopy (XPS)

X-ray photoelectron spectroscopy (XPS) was performed to examine the surface chemical composition of the catalysts. A PHI-VersaProbe III XPS spectrometer equipped with Al source. For the XPS survey spectra, data were acquired with a pass energy (Ep) of 280 eV and an energy

step (Es) of 1.0 eV, while high- resolution spectra were obtained using Ep =26 eV and Es = 0.1 eV. The XPS spectra were analyzed using CasaXPS software (CasaXPS Software Ltd., USA). Binding energies (B.E.) were referenced to the C 1 s peak at 284.8 eV, and high-resolution envelope curves were fitted using mixed Lorentzian–Gaussian curves.

2.4 Micropyrolyzer

The experiments were conducted using a single-shot tandem micro-pyrolysis facility (Rx-3050tr, Frontier Labs, Japan) coupled with two-dimensional gas chromatography (GC × GC) and a separate, customized multi-column GC (Trace 1300) for light gas analysis. The GC inlet and reactor pressures were maintained at ~2.7 bara, with a column flow rate of 0.75 mL/min. For non-catalytic pyrolysis experiments, a single-reactor configuration was used, with a pyrolysis temperature of 600 °C applied throughout. For catalytic pyrolysis tests, a dual-reactor configuration was employed, where both reactors were set to 600 °C for consistency across experiments. These temperatures are optimal to minimize char yield during PET pyrolysis [49]. A detailed description of the micro-pyrolysis unit is described elsewhere and [51] illustrated in **Figure S1** and **Figure S2**.

In each experiment, a plastic mixture totaling 0.4 mg with PET to LDPE ratios of 3:1, 1:1, and 1:3 was prepared in an Ecocup-SF (80 µL) on a microbalance, covered with quartz wool, and loaded into the double-shot sample holder with an Eco-Stick SF (30 mm). The sample was then dropped into the pre-heated pyrolysis reactor at 600 °C. Helium was used as the carrier gas (20 mL/min) to transport volatiles into the second reactor, which was also maintained at 600 °C. This reactor contained a fixed catalyst bed inside an 8-cm-long quartz tube with an inner diameter of 2.85 mm. The catalysts were secured between quartz wool plugs and positioned within the isothermal zone of the tandem reactor [5].

The catalyst-to-plastic (C/P) ratio was maintained at 20 (wt./wt.) for all catalysts. This ratio, previously optimized for parent HZSM-5 in our studies on upgrading polyethylene and polypropylene pyrolysis vapors for light olefin production [3, 5], was retained here to assess the effect of PET presence in the feed on product distribution under identical conditions. All catalysts were mixed with inert α-alumina to ensure a constant bed height of 10 mm, resulting in a catalyst-vapor contact time of 146 ms, defined as the total time that pyrolysis vapors remain in contact with the catalysts [5, 52].

2.5 Product Analysis

The effluent from the reactor section of the micropyrolyzer facility was characterized and quantified using the FID detector on a GC × GC (TRACE GC ULTRA) and a separate, customized multi-column GC (Trace 1300). The analytes were initially trapped in the first part of the analytical column via a cryo-focusing device (MJT-1035E) that utilized a jet of liquid nitrogen (-190 °C). This cryo-trap held the products for 5 minutes while the GC oven was maintained at -40 °C through cryogenic cooling. After 5 minutes, the nitrogen flow was stopped, and the cooled area of the column was rapidly heated to match the oven temperature (-40 °C). Using a cryo-trap facilitates rapid analyte desorption and improves peak separation, particularly for low-boiling-point compounds. Before entering GC × GC separation, the column flow was branched to a customized multi-column GC (Trace 1300) for light gas analysis. The GC oven was held at -40 °C for 15 minutes, then ramped to 302 °C at a rate of 3 °C/min. A Sep-Solv flow modulator, with a modulation time of 4.8 seconds and a flush time of 1 second, was positioned between the first and second-dimension columns. The non-polar MXT-1 column (30 m, ID = 0.25 mm) served as the first dimension column, separating compounds by boiling point, while the second dimension mid-polar ZB-35HT column (5 m, ID = 0.25 mm) provided separation based on polarity. The second column outlet flow was split into a TOF/MS and an FID for volatile identification and quantification.

For PET pyrolysis experiments, the FID response was calibrated by pyrolyzing benzoic acid at 300 °C with three different loadings (29 µg, 50 µg, 60 µg), where it solely volatilizes as benzoic acid. FID calibration was performed using iso-butane (5%, balance He) for LDPE pyrolysis [5]. The customized multicolumn GC was calibrated utilizing the responses on TCD and PDD detectors with two separate calibration mixtures procured from AirProducts containing CH_4, CO, CO_2, ethylene, ethane, propylene, propane, and 1,3-butadiene. The FID and TCD calibrations, excluding CO and CO_2 yields (which do not appear in the FID chromatogram), were cross-validated, yielding consistent data. Product identification was achieved using a BenchTOF-Select™ (Markes, United Kingdom) MS, scanning over an m/z range of 20–600 at 70 eV. MS spectra were compared against the NIST library database (MS Search 2.2), with data processing completed via GC Image software. Product yields were then calculated using the molar response factor (MRF) approach [53] based on quantified iso-butane for each run. A detailed description of MRF is provided supplementary information.

The cryogenic trap did not capture light gases such as methane and CO, which were sent to customized multi-column GC (Trace 1310). Once the cryo-trap was deactivated, C_2-C_4 components were first eluted, followed by the well-separated C_{5+} products. Notably, any ethane and propane present in the products would co-elute with ethylene and propylene, although the yields of ethane and propane are presumed to be low, leading to only a minor overestimation of ethylene and propylene yields. Prior studies support this conclusion [3, 5, 8] and several observations: first, MS identification of product peaks indicated clear matches for ethylene and propylene. Additionally, the low yield of C_1 and C_4 alkanes (<1.5 wt%) suggests minimal "over cracking" and hydrogen transfer due to short vapor residence times and moderate upgrading temperatures. Consequently, ethane and propane yields are expected to be minor. Moreover, the TCD peak for ethane was only noticeable when LDPE was pyrolyzed with unmodified

HZSM-5, where the maximum ethane yield in pure LDPE pyrolysis reached only 1.3 wt.%. Propane was undetectable by TCD due to its negligible concentration.

The synergistic effect of PET and LDPE co-pyrolysis was examined following the method described by Toraman's group [13, 44]. In this approach, the yields of individual products obtained from PET and LDPE pyrolysis were compared with those obtained under co-pyrolysis conditions. Synergy%(x) was calculated using Equation 1, where x represents the compound of interest, $y(x)_{actual}$ is the yield (wt.%) of compound x obtained from co-pyrolysis, $y(x)_{PET}$ and $y(x)_{LDPE}$ are the yields of compound x obtained during individual PET and LDPE pyrolysis, respectively, while w_{PET} and w_{LDPE} are the mass fractions of PET and LDPE in the feed. For example, if the pyrolysis of a 400 µg PET-LDPE mixture with a 1:1 PET-to-LDPE ratio results in a 50% synergy effect for C_5-C_{11}, it means that co-pyrolysis produces 50% more C_5-C_{11} (by weight) than the total C_5-C_{11} yield from the separate pyrolysis of 200 µg PET and 200 µg LDPE. Conversely, a negative synergy value indicates that co-pyrolysis generates less C_5-C_{11} than the combined yields from the individual pyrolysis of PET and LDPE. If the synergy value is 0%, it means no synergistic effect is observed, and co-pyrolysis produces the same C_5-C_{11}yield as the sum of the separate pyrolysis processes.

$$Synergy\%(x) = \frac{y(x)_{actual} - (w_{PET} * y(x)_{PET} + w_{LDPE} * y(x)_{LDPE})}{w_{PET} * y(x)_{PET} + w_{LDPE} * y(x)_{LDPE}} * 100 \qquad (1)$$

3 Results and Discussion

3.1 Catalyst properties

The crystallinity of the catalysts was examined using X-ray diffraction (XRD), as shown in **Figure 1**. All catalysts exhibited two prominent peaks at 7.9° and 8.8°, corresponding to the [0 1 1] and [2 0 0] crystal planes of HZSM-5, and five characteristic peaks in the range of 22–25°, specifically at 23.2°, 23.4°, 23.8°, 24.1°, and 24.5°, which correspond to the[5 0 1], [0 5 1], [1 5 1], [3 0 3], and [1 3 3] crystal planes of HZSM-5 [54]. The addition of Ga and Zn did not alter the spectra, preserving the characteristic peaks of the parent HZSM-5 and confirming that the MFI structure remained intact [55]. Furthermore, there were no observable peaks for impregnated metal oxides, as a result of Ga_2O_3 and ZnO low concentration and small particle sizes or their amorphous nature. This aligns with findings reported in the literature for similar catalysts [28, 35, 55]. However, the characteristic peaks in the 22–25° range decreased with the addition of Zn and Ga, exhibiting a reduction in relative crystallinity [28] to 85% and 62%, respectively, compared to the parent catalyst (100%).

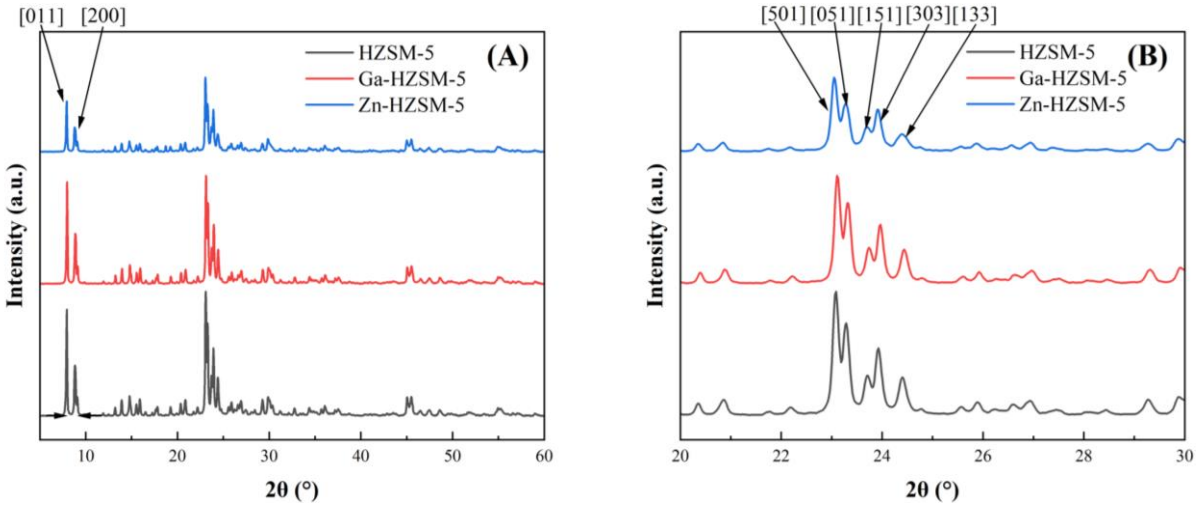

Figure 1. XRD patterns of parent HZSM-5, Ga-HZSM-5, and Zn-HZSM-5

N_2-physisorption is known to underestimate absolute micropore volumes compared to argon or CO_2, due to nitrogen's quadrupole moment and kinetic limitations in accessing narrow pores. However, when pretreatment and measurement conditions are kept consistent across samples, the method provides reliable relative trends suitable for comparative analysis. This is demonstrated in **Figure S3**, where the application of an identical protocol to all samples shows that the BET surface areas and total pore volumes of Ga-HZSM-5 and Zn-HZSM-5 are comparable to those of the parent HZSM-5 catalyst (see **Table 1**). In contrast, a different trend was observed in our previous study on phosphorus-impregnated HZSM-5: although N_2 physisorption captured the decrease in microporosity, the absolute loss was less pronounced than that measured by Ar physisorption, which is generally considered more accurate for micropore analysis [8, 56].

All studied catalysts displayed typical microporous characteristics, evidenced by type I isotherms (**Figure S3**), which are commonly associated with materials possessing extremely fine micropores [57]. Thus, the micropore surface area and micropore volume constitute most of the specific surface area and pore volume (**Table 1**). Moreover, SEM-EDX analysis shows that Ga and Zn concentrations are 1±0.5 wt.% and 0.7±0.4, and the Si/Al molar ratio remains unchanged with Ga or Zn modifications (**Figure S4**).

Table 1. Physical properties of the catalysts.

Samples	S_{BET} [a] ($m^2 \cdot g^{-1}$)	S_{micro} [b] ($m^2 \cdot g^{-1}$)	S_{ext} [c] ($m^2 \cdot g^{-1}$)	V_{total} [d] ($cm^3 \cdot g^{-1}$)	V_{micro} [e] ($cm^3 \cdot g^{-1}$)
HZSM-5	419.5	392.9	26.7	0.23	0.17
Ga-HZSM-5	411.0	384.5	26.5	0.22	0.16
Zn-HZSM-5	416.6	398.8	17.8	0.23	0.17

[a] BET surface area, [b] t-Plot Micropore Area, [c] t-Plot external surface area, [d] Single point adsorption total pore volume at $p/p° = 0.99$, [e] t-Plot micropore volume.

The results of NH_3-TPD are shown in **Figure 2**. Two distinct desorption peaks are observed: one in the range of 200–300 °C, corresponding to weak acid sites (primarily Si–OH), and another between 300–500 °C, associated with strong acid sites (Si–OH–Al) [58]. To quantify these sites, the TPD curves were deconvoluted into low- and high-temperature peaks, representing weak and strong acidity, respectively. The corresponding acid site concentrations are summarized in **Table 2**. NH_3-TPD is not a precise descriptor of acid strength since it can conflate acid strength with confinement and diffusional effects. However, it can still provide useful comparative insights when applied to catalysts with the same framework structure and Si/Al ratio, as in our study. N_2 physisorption and XRD analyses confirmed that Zn and Ga modification did not significantly alter the crystal structure or textural properties of HZSM-5. Therefore, we interpreted the observed changes in the NH_3 desorption profiles primarily as differences in acidity, assuming similar confinement effects across the samples. The total acidity of HZSM-5 decreased upon modification with Ga and Zn. This reduction can be attributed to the interaction of well-dispersed GaO_x and ZnO_x species with extra-framework Al, which alters the nature of the parent acid sites and lowers both total acidity and acid strength. Notably, the main change was observed in the distribution of acid sites. Compared to parent HZSM-5, the number of weak acid sites in Ga-HZSM-5 increased from 0.109 to 0.155 mmol NH_3/g, while the number of strong acid sites decreased from 0.321 to 0.245 mmol NH_3/g. This shift may result from the partial exchange of Brønsted acid sites and the formation of new Ga-associated Lewis acid sites [30, 35]. Similarly, Zn impregnation led to a further decrease in the number of strong acid sites while increasing the number of weak acid sites. This can be explained by the interaction of ZnO_x species with Brønsted protons, forming $ZnOH^+$ species and reducing the population of strong acid sites [59]. Additionally, Zn can also substitute protons from Al–OH groups, forming Al–O–Zn acid sites, which are classified as weak-to-

medium acid sites (reflected in the NH_3 desorption peak at 200–300 °C), thereby increasing the number of weak acid sites [28, 60].

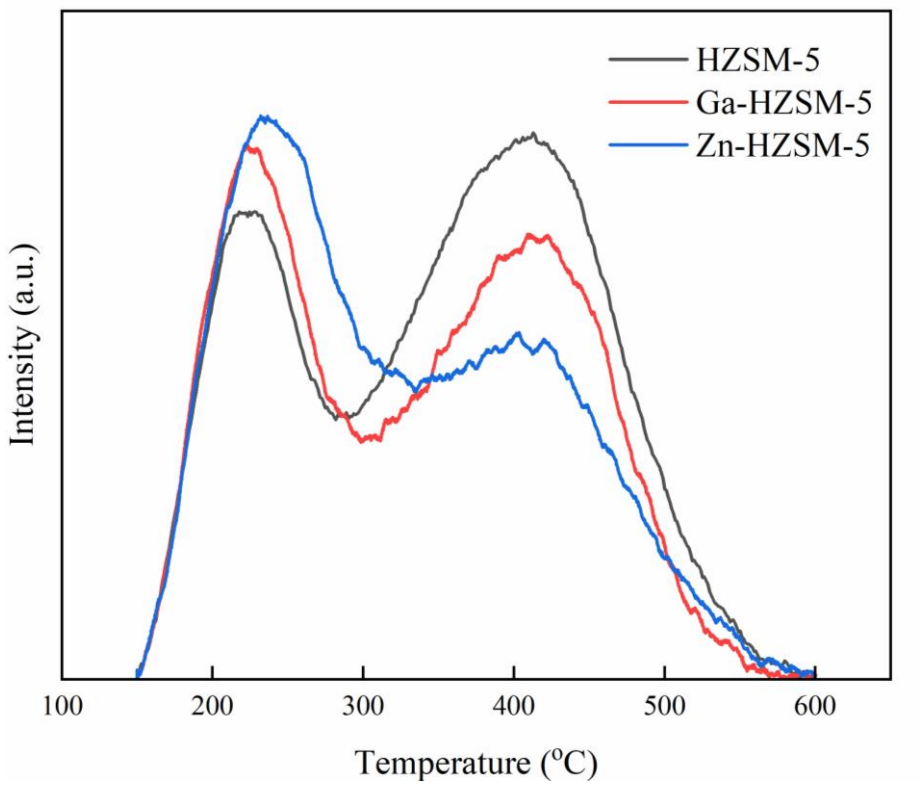

Figure 2. NH_3-TPD profiles of HZSM-5, Ga-HZSM-5 and Zn-ZHSM-5.

Table 2. Acidic properties of the studied catalysts.

Samples	Total acidity (mmol NH_3/g)	Weak acidity (mmol NH_3/g)	Strong acidity (mmol NH_3/g)	Strong to Weak acid site ratio (Strong / Weak)
HZSM-5	0.456	0.125	0.331	2.64
Ga-HZSM-5	0.401	0.153	0.248	1.62
Zn-HZSM-5	0.398	0.171	0.227	1.32

XPS was used to quantify the surface elemental composition of the catalysts and to elucidate the chemical states of the impregnated Ga and Zn species. **Table 3** summarizes the relative

atomic concentrations obtained from the XPS analysis. In the Zn-modified sample, the Zn signal was detected near the instrumental detection limit, suggesting that most of the Zn is not concentrated on the external surface but might have migrated deep inside the micropores and bulk of the material [35]. Despite this low surface concentration, the Zn $2p_{3/2}$ region was recorded with high energy resolution (0.1 eV step; **Figure 3**A). Two distinct Zn species were identified, with binding energies (BE) of ~1023 eV and ~1024 eV. The lower binding energy peak is attributed to ZnO, while the higher binding energy peak is assigned to zinc species interacting with the zeolite framework, specifically $ZnOH^+$ (Zn-Lewis acid sites) formed through the interaction of Zn with Brønsted acid sites on the zeolite [61]. Peak area analysis showed that 20% of the surface zinc was present as ZnO, while the remaining 80% existed as $ZnOH^+$. Notably, Niu et al. performed X-ray absorption fine structure (XAFS) analysis on Zn-impregnated HZSM-5 prepared using a similar method and similarly reported that only a small fraction (~28%) of Zn was present as ZnO, with the majority in the form of $ZnOH^+$. They also observed nano-sized Zn species dispersed within the zeolite channels. On the other hand, when ion exchange was used as the modification method, the resulting Zn species were completely well-dispersed as $ZnOH^+$, with no ZnO detected by XPS [61]. The Al 2p spectrum was also recorded with high energy resolution (**Figure S5**); however, it did not show a significant difference compared to the parent catalyst. This could be attributed to the relatively low surface concentration of Zn atoms in comparison to Al atoms.

Table 3. Atomic concentrations of HZSM-5, Ga-HZSM-5 and Zn-HZSM-5.

	Atomic Concentration (%)					
Catalyst	C	O	Al	Si	Ga	Zn
HZSM-5	18.7	57.2	1	23.1	-	-
Ga-HZSM-5	10.3	62.8	1.1	24.8	1	-
Zn-HZSM-5	16.9	58.1	1	23.8	-	0.2

Ga displays a markedly stronger XPS signal than Zn, suggesting that a substantial fraction of the gallium resides on the external surface or at the pore mouths of the zeolite crystals. This is consistent with literature reports, as wetness impregnation of Ga typically results in its deposition predominantly on the catalyst surface [62]. To probe the chemical state of these species, the Ga $2p_{3/2}$ region was recorded at high energy resolution (0.1 eV step; **Figure 3B**). The envelope centered at 1118.7 eV for Ga $2p_{3/2}$ [63] is resolved into two components at 1118.5 eV and 1119.8 eV [64]. The lower-binding-energy peak (1118.5 eV) is assigned to extra-framework GaO_x species as GaO^+ ions anchored to framework Al via Ga–O–Al linkages or present in small Ga–O–Ga domains which experience partial electron donation from neighboring oxygens and therefore exhibit a slight negative shift relative to bulk Ga_2O_3 [65]. The higher-binding-energy component (1119.8 eV) corresponds to small Ga_2O_3 clusters. Peak area analysis shows that ~75 % of the surface Ga is associated with the lower-binding-energy GaO_x component.

To corroborate the presence of GaO_x species interacting with extra-framework Al high resolution Al 2p spectra were collected for the parent and Ga-modified HZSM-5 samples (**Figure S6**). The integrated Al 2p peak areas are essentially the same in both catalysts, confirming that Ga introduction does not alter the overall Al surface concentration. In contrast, the spectral shape changes markedly: the Ga-HZSM-5 spectrum is broader and centered at 74.3 eV, ~ 0.8 eV lower than the narrower Al 2p peak of the parent zeolite at 75.1 eV. This negative binding energy shift is consistent with an increase in local electron density at Al sites caused by nearby Ga^{+3} species sharing framework oxygens (Ga–O–Al linkages). The electronic donation from Ga lowers the ionization energy of Al, broadens the envelope by creating a distribution of Al environments, and thus provides further evidence for GaO_x–Al interactions, which is also observed in the study of Jahangiri et al. [66].

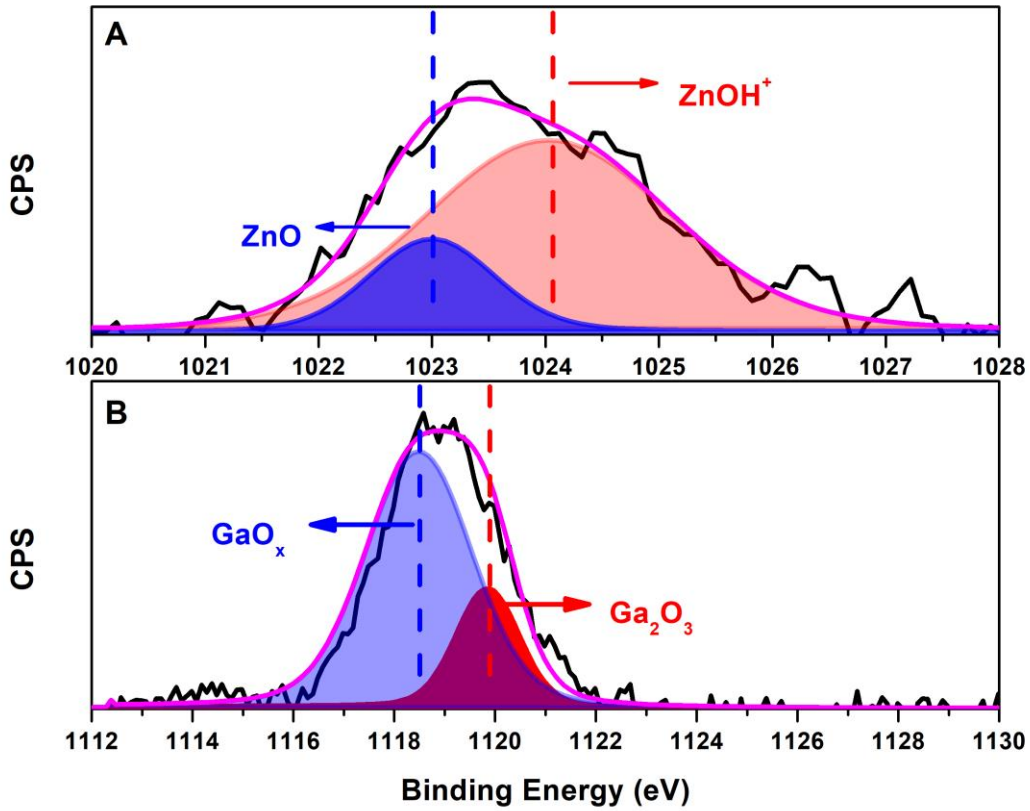

412

413 **Figure 3.** XPS spectra of (A) Zn $2p_{3/2}$ for Zn-HZSM-5 and (B) Ga $2p_{3/2}$ for Ga-HZSM-5.

414 **3.2 Thermal Pyrolysis**

415 Previous pyrolysis screening using thermogravimetric analysis (TGA) demonstrated that
416 pyrolysis of PET at 600 °C results in a minimal solid char formation, accounting for 16.8±1
417 wt.% of the total feed [49]. Further details regarding the TGA methodology and results are
418 provided in the Supplementary Information. Consequently, 600 °C was selected as the optimal
419 pyrolysis temperature for all experiments to maximize the recovery of valuable pyrolysis oil
420 (PyOil) and pyrolysis gas (PyGas).

421 The primary products of PET pyrolysis at 600 °C are illustrated in **Figure 4**. The major gaseous
422 products were CO_2 (20.0±2 wt.%), CO (6.6 ±0.2 wt.%), acetaldehyde (8.1±0.7 wt.%), and
423 ethylene (2.4±0.2 wt.%), along with trace amounts of ethane and propylene (<0.5 wt.%).

Overall, gas yields constituted 37.9±0.8 wt.% of the pyrolysis products. The condensable product yield was 45.3±2.6 wt.%, with benzoic acid (22.8±0.9 wt.%), benzene (5.7±0.7 wt.%), and vinyl benzoate (3.7±0.2 wt.%) being the predominant components. Relatively lower amounts of styrene, toluene, and divinyl terephthalate (DVT) were also detected. Additionally, the condensable fraction contained other ketones and aldehydes in smaller quantities, as detailed in **Table S3-S7**. Notably, terephthalic acid was absent in the pyrolysis products at 600 °C, likely due to rapid decarboxylation into benzoic acid and benzene [22].

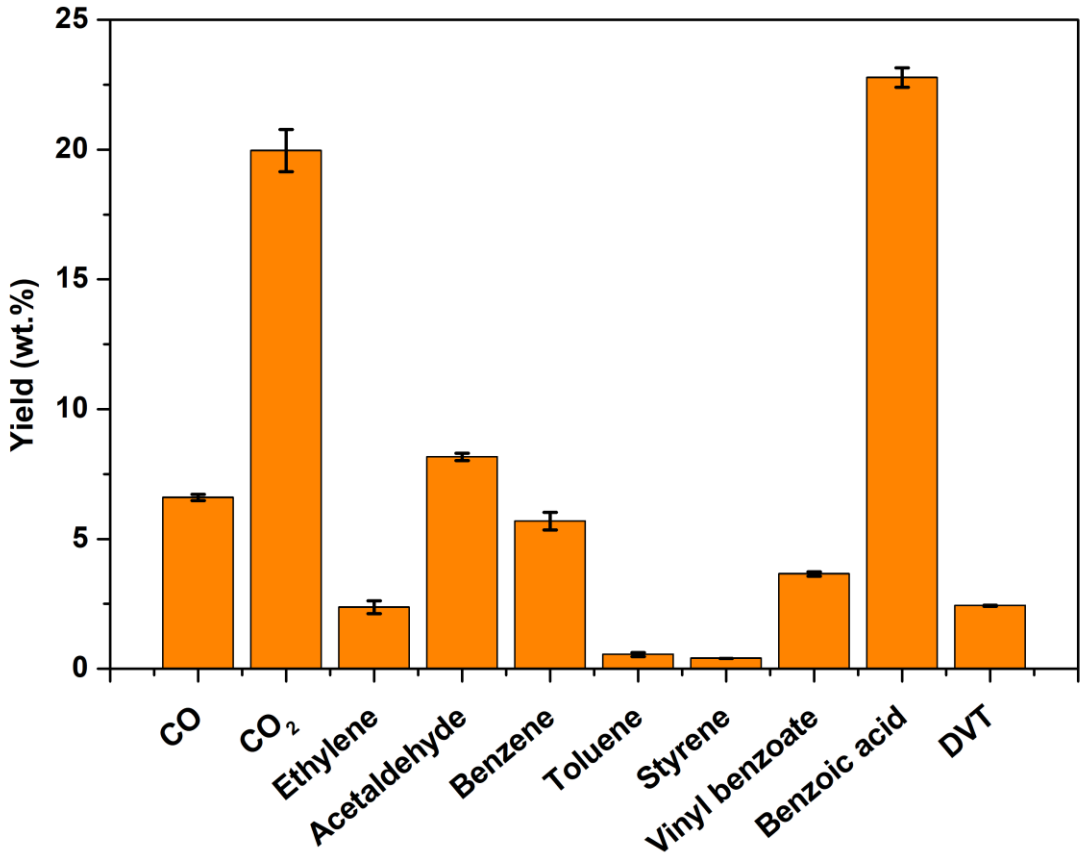

Figure 4. Product distribution from the thermal pyrolysis of PET at 600 °C.

Figure 5 illustrates the reaction pathways for the major products formed during the pyrolytic cracking of PET, with the radical mechanisms proposed by Andrea et al. highlighted using red arrows [49]. Numerous studies report that the cleavage of ester bonds through β-hydrogen

transfer to the carbonyl carbon produces carboxyl and vinyl end groups, forming TPA and vinyl benzoate (VB) and [13, 22, 67]. Subsequent decarboxylation and decarbonylation of TPA and VB yield benzoic acid, acetophenone, CO_2, and CO. The high yield of acetaldehyde is attributed to the presence of hydroxyethyl end groups. According to Kumagai et al., these hydroxyethyl end groups form carboxyl end groups and acetaldehyde via a seven-membered-ring transition state [16, 22]. The notable CO_2 yield explains the absence of TPA in the product spectrum during PET pyrolysis at 600 °C. The decarboxylation of TPA and benzoic acid is the primary contributor to CO_2 generation, indicating that TPA undergoes rapid decarboxylation at this temperature. Similarly, high benzene yields suggest the decarboxylation of benzoic acid, further contributing to CO_2 production. Ethylene was also detected in relatively lower quantities, and literature suggests its formation occurs through an intermolecular reaction where vinyl-terminated carboxylate units and PET units interact, forming an eight-membered cyclic transition state that produces ethylene and carboxyl end groups [68].

Benzoic acid can also undergo dehydration and dehydrogenation reactions to produce biphenyl, fluorenone, and benzophenone, observed in relatively small amounts during pyrolysis at 600 °C. Water was also detected in the MS spectra, although its corresponding TCD peak was negligible compared to other major products (CO, CO_2, and ethylene). These minimal yield of water, along with the low concentrations of biphenyl, fluorenone, and benzophenone, indicate that dehydration and dehydrogenation reactions were less favored than decarboxylation at 600 °C. Furthermore, the lower yields of decarbonylation products compared to decarboxylation products suggest that decarboxylation was the dominant reaction pathway for PET pyrolysis at this temperature. This conclusion is further supported by the low CO yields observed in the experiments.

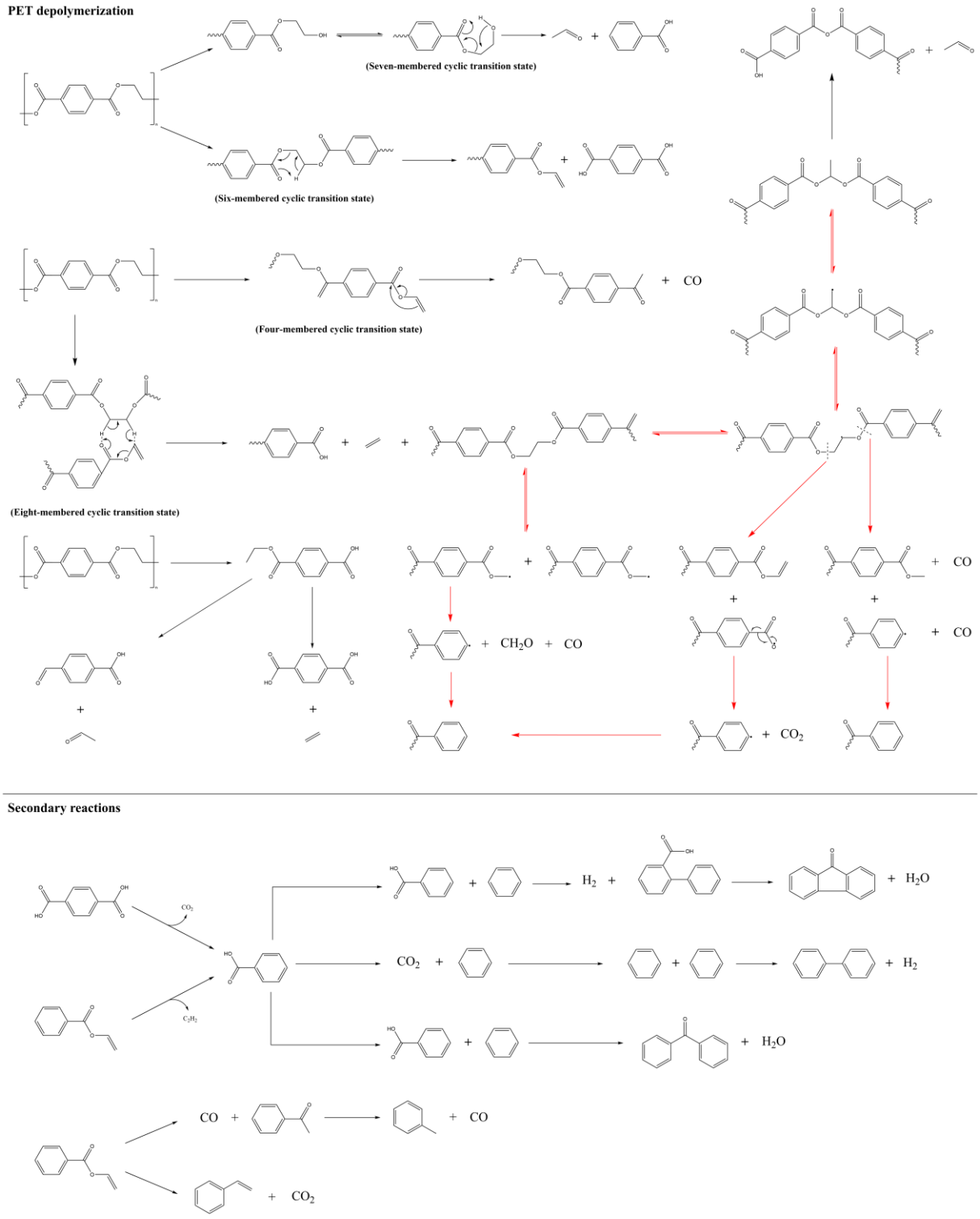

Figure 5. Proposed formation pathways of major products during PET pyrolysis via molecular (black) and radical (red) mechanisms. Adapted from references [13, 22, 49, 67].

The effect of LDPE-PET co-pyrolysis on product distribution was explored by pyrolyzing virgin LDPE and PET-LDPE mixtures with varying PET to LDPE ratios (3:1, 1:1 and 1:3) at

600 °C, allowing for a detailed examination of the resulting product spectrum. Pyrolysis of LDPE leads to a broader product spectrum than PET, yielding products with a wider carbon number range. Hence, besides methane, ethylene, and propylene, other hydrocarbons were grouped as butenes, naphthenes, BTX, C_5-C_{11}, C_{12}-$C_{20,}$ and C_{21}-C_{31} aliphatics and shown in **Figure S7**.

Figure 6 shows the co-pyrolysis results of PET-LDPE mixtures, along with references for pure PET and pure LDPE. For ease of comparison across different PET to LDPE ratios, all oxygen-containing compounds other than CO and CO_2 were grouped under "oxygenated" compounds. The carbon, hydrogen, and oxygen balances for the experiments are presented in **Table S8 and Table S9**. As expected, full closure of the C and O balances was not achieved in any of the runs. For PET and PET-dominated mixtures, the primary cause of this discrepancy is char formation, which, as suggested by the results, consists predominantly of carbon. Additionally, small amounts of heavy condensable compounds containing C, H, and O may have formed but were not detected by GC due to their high boiling points (≥350 °C). In the case of PET pyrolysis, the missing mass fraction (~18–20 wt.%) aligns closely with the char yield (16.8 wt.%) determined by TGA, indicating that the majority of the unaccounted C and O remain in the solid residue. For LDPE and LDPE-rich mixtures, the primary source of the missing C and H fractions is likely the formation of heavy hydrocarbons (C30+), which exceed the detection range of the GC × GC method employed.

Product quantification revealed that the yields of CO, CO_2, oxygenated compounds, and aromatics increased proportionally with PET content, while lower PET-to-LDPE ratios resulted in decreased yields of these species. The most notable change was observed in the oxygenated compounds: introducing LDPE into the PET feed at a PET:LDPE ratio of 3:1 reduced the oxygenated compound yield from 45.2±2.7 wt.% to 31.6±0.4 wt.%, and further increasing the

LDPE content to a PET:LDPE ratio of 1:3 dramatically decreased it to 5.3±0.2 wt.%. Conversely, the yields of C_2-C_4 olefins and C_5-C_{31} aliphatic hydrocarbons were proportional to the LDPE content. For example, decreasing the PET:LDPE ratio from 3:1 to 1:3 significantly promoted C_5-C_{31} aliphatic formation, surpassing the yields observed in pure LDPE pyrolysis. This suggests a synergistic effect between PET and LDPE during co-pyrolysis.

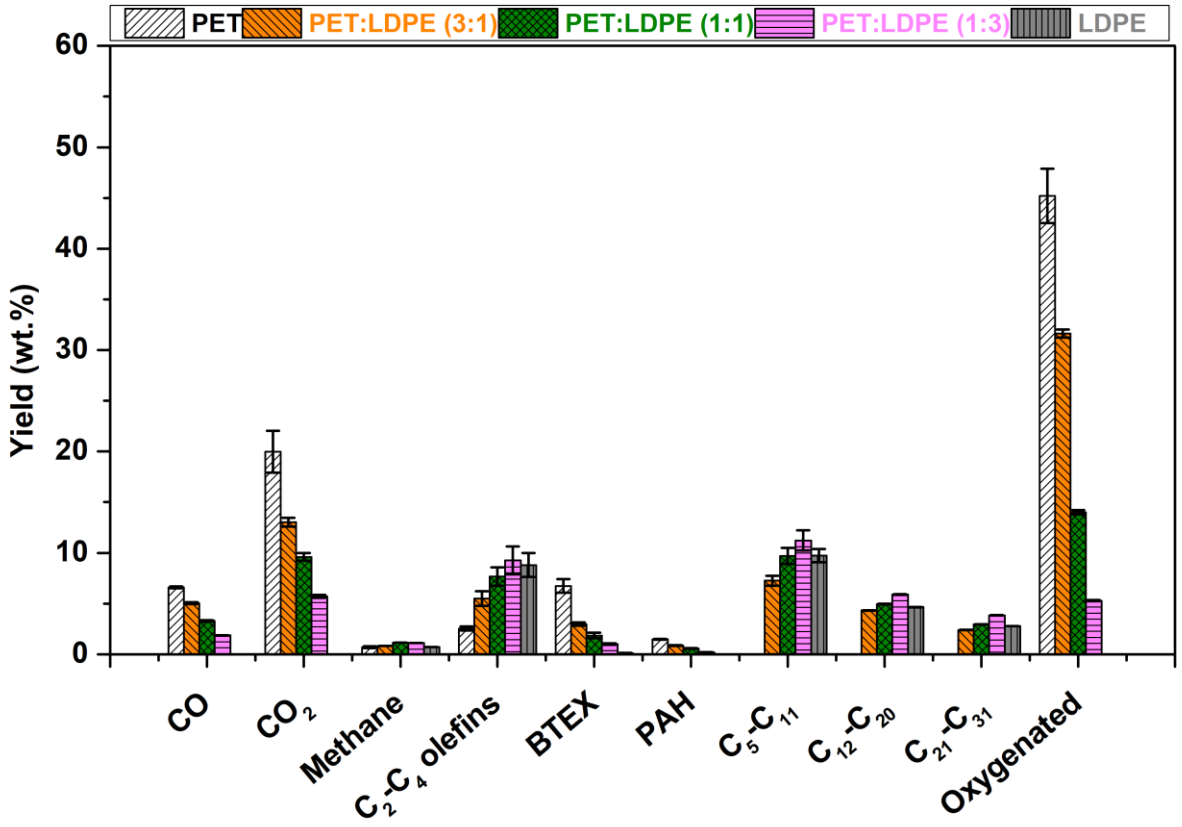

Figure 6. Effect of PET-to-LDPE ratio during co-pyrolysis at 600 °C on product distribution.

The synergistic effect between PET and LDPE on product distribution at varying PET to LDPE ratios was further analyzed using the method proposed by Okonsky et al. [13, 44] and illustrated in **Figure 7**. The results indicate that the co-pyrolysis of PET and LDPE did not exhibit a significant synergistic effect on CO and CO_2 production. On the other hand, increasing LDPE

amount in pyrolysis feed has led to a negative synergy for other oxygenated compounds, primarily acetaldehyde, benzoic acid, and vinyl benzoate. This suggests that co-pyrolysis positively influences PyOil quality by reducing its oxygen content. The results indicated a negative synergistic effect on BTX and polycyclic aromatic hydrocarbon (PAH) production, despite the observed decrease in oxygenated compounds. Intuitively, a positive synergy in aromatic production would be expected, as their formation is typically linked to the decarboxylation of organic acids leading to aromatics. This could be explained by the formation of heavy oxygenated compounds and/or PAHs that cannot be detected with the column configuration employed in our GC × GC, as the maximum reachable oven temperature was limited to 300 °C. The internal standard suggests that over 45 wt.% of heavy products are formed at 1:1 PET to LDPE ratio.

The co-pyrolysis of PET and LDPE showed a positive synergistic effect on the production of C_5-C_{31} aliphatic, suggesting that adding PET to the LDPE feed facilitates LDPE cracking. Increasing the PET concentration in the mixture further enhances these cracking reactions, with the synergy for C_{12}-C_{20} aliphatic production reaching 272%. This effect is likely due to the increased concentration of PET derived-radicals in the gas phase at 600 °C [49, 69, 70], which enhances LDPE cracking.

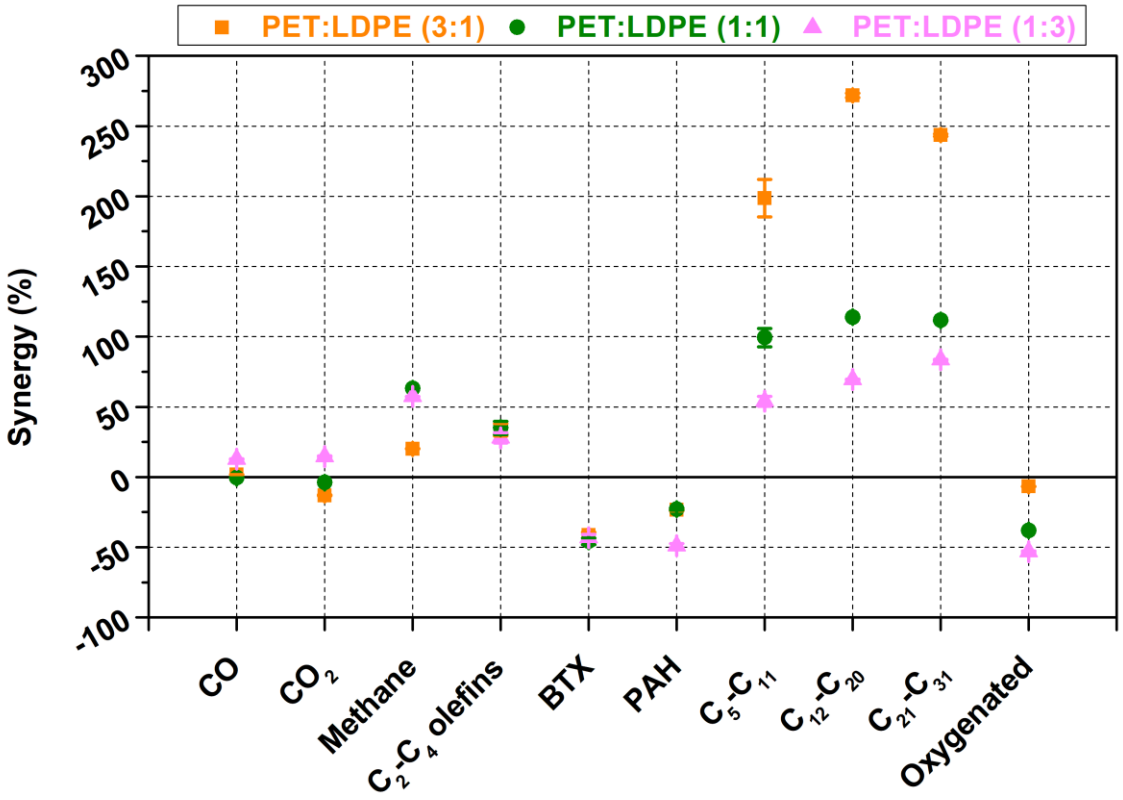

Figure 7. Effect of PET:LDPE ratio on synergy for co-pyrolysis of PET and LDPE at 600 °C.

3.3 Catalytic Upgrading of PET Pyrolysis Vapors

The effect of catalyst modification on upgrading PET pyrolysis vapor in a close-coupled second reactor was investigated by cracking pyrolysis vapors in a secondary catalytic reactor at 600 °C. The yields of the major product groups are shown in **Figure 8**. All catalysts exhibited excellent activity for decarboxylation and aromatization, as no detectable amounts of oxygenated products other than CO and CO_2 were observed in any of the catalytic tests. The introduction of catalysts increased CO_2, CO, and aromatic yields due to enhanced decarboxylation and decarbonylation reactions.

Among the catalysts studied, HZSM-5 exhibited the lowest BTX selectivity at 28.3±0.7 wt.% but the highest yields of C_2-C_4 olefins (10.5±1.4 wt.%) and other monoaromatics (1.8±0.1 wt.%). The increased yields of C_2-C_4 olefins and alkylated benzenes suggest that parent HZSM-5 is relatively less selective for decarboxylation and decarbonylation reactions, promoting alkylation and aromatization to a greater extent compared to Ga- and Zn-promoted catalysts.

Ga impregnation on HZSM-5 improved the selectivity for BTX, increasing the yield from 28.3±1.5 wt.% to 31.9±0.8 wt.% compared to the parent HZSM-5. However, there was a noticeable rise in polyaromatic yields, which increased from 4.2±0.2 wt.% to 6.5±0.2 wt.% with Ga promotion. This could be attributed to enhanced hydrogen transfer reactions facilitated by the formation of GaO_x species, which introduce new Lewis acid sites on the catalyst surface [71]. The observed reduction in C_2-C_4 olefin yields is likely due to the increased extent of aromatization, wherein light olefins are converted to aromatics, potentially co-catalyzed by neighboring Brønsted acid sites. Notably, Brønsted acid sites are known to promote the cyclization steps during aromatization [72], and a synergistic interaction between Ga species and nearby Brønsted acid sites has been reported to play a critical role in the dehydrogenation and aromatization of ethylene [73]. Therefore, it is essential to avoid excessive coverage of Brønsted acid sites by GaO_x or $ZnOH^+$ species, as this may impair the overall catalyst performance.

The highest selectivity towards BTX was achieved with Zn-HZSM-5, where Zn impregnation further increased BTX selectivity to 33±0.8 wt.% while minimizing polyaromatic formation to 3.5±0.1 wt.%. This difference can be attributed to the nature, concentration, and spatial distribution of the active sites. GaO_x species might promote hydrogen transfer reactions more effectively than ZnOH+, thereby facilitating the conversion of mono-aromatics into larger polyaromatic structures. In contrast, Zn-associated Lewis acid sites tend to favor BTX

554 formation rather than PAH, compared to Ga-modified active sites [74]. Secondly, XPS analysis
555 showed a significantly higher surface concentration of Ga relative to Zn. This elevated Ga
556 content may lead to excessive hydrogen abstraction, which in turn promotes the formation of
557 PAHs. In contrast, significantly lower surface concentration of Zn suggests that a substantial
558 fraction of the Zn species likely migrates into the zeolite micropores or the or the bulk phase of
559 the catalyst. However, given the significant changes observed in acid site distribution and
560 product selectivity relative to the parent catalyst, it is highly likely that the majority of ZnO_x
561 species migrated deep into the zeolite channels rather than accumulating in the bulk phase. Zn
562 ,located in the bulk, would not be expected to induce such pronounced catalytic effects. This
563 suggests that the spatial distribution of active sites is a key factor. Hence, low Zn concentration
564 detected on the external surface further supports the hypothesis that a substantial portion of Zn
565 resides within the zeolite micropores, a conclusion consistent with the XAFS findings reported
566 by Niu et al. [61]. Consequently, if Zn-containing active sites are primarily responsible for
567 aromatization, the pore confinement effect within the zeolite channels may more effectively
568 suppress PAH formation compared to the Ga-modified catalyst, where the active sites are
569 predominantly external and thus less influenced by confinement. This trend becomes even more
570 pronounced during the co-pyrolysis of PET and LDPE, as discussed in the following section.
571 Another notable difference observed with Zn-HZSM-5 was the higher generation of CO_2
572 (27.6±0.9 wt.%) and slightly lower CO production (10.0±0.2 wt.%) than Ga-HZSM-5. This
573 indicates that Zn-HZSM-5 favors decarboxylation reactions over decarbonylation reactions
574 more than Ga-HZSM-5.

575 However, the differences in BTX, PAH, CO, and CO_2 yields among the three catalysts are
576 relatively small (~1–3 wt.%). This is primarily attributed to the inherently high activity of the
577 parent HZSM-5 for decarboxylation and decarbonylation reactions, which limits the extent of
578 improvement achievable through metal modification. In contrast, the catalytic effects of Ga and

Zn become significantly more pronounced during LDPE pyrolysis and PET–LDPE co-pyrolysis.

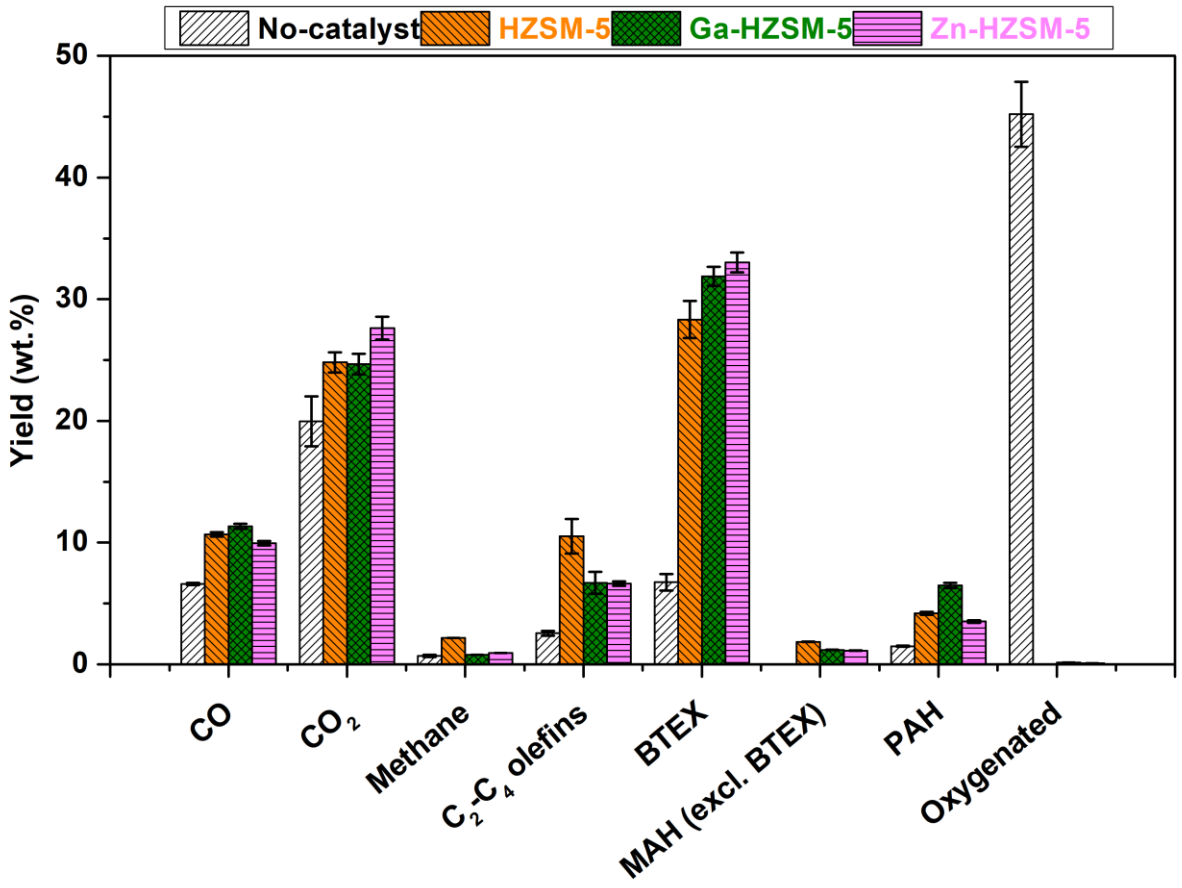

Figure 8. Catalytic upgrading of PET pyrolysis vapors over HZSM-5, Ga-HZSM-5, and Zn-HZSM-5 at 600 °C.

3.4 Effect of PET and LDPE ratio on catalytic co-pyrolysis vapor cracking on product distribution

The impact of PET and LDPE co-pyrolysis on product distribution was analyzed, focusing on industrial applicability by categorizing the products into PyGas and PyOil. Pyrolysis char was excluded from graphical representations, as it does not reach the catalytic reactor; however, it

was included in mass closure calculations. PyGas was defined as the gaseous products consisting of CO, CO_2, methane, and C_2-C_4 olefins and paraffins and acetaldehyde while PyOil encompassed C_{5+} aliphatic compounds, BTX, poly-aromatics, and oxygenates. The influence of varying PET to LDPE ratios on PyGas and PyOil yields is depicted in **Figure 9**.

Compared to thermal pyrolysis, all catalysts produced higher PyGas yields across all PET-to-LDPE ratios. This can be attributed to two primary factors. First, the catalysts enhanced cracking reactions, shifting the product distribution toward lighter compounds, particularly C_2–C_4. Second, they were highly effective in deoxygenating reactions, resulting in increased formation of CO and CO_2. Regarding PyOil yield, under all co-pyrolysis conditions, the Ga- and Zn-modified catalysts produced more oil, while the parent HZSM-5 catalyst yielded less PyOil compared to thermal pyrolysis. This trend reflects the ability of Ga and Zn modifications to enhance aromatization reactions while still generating relatively high amounts of light olefins compared to thermal pyrolysis, thus increasing the PyOil fraction. In contrast, HZSM-5 exhibited excellent cracking activity, strongly favoring light olefin production along with CO and CO_2 formation, which boosted the PyGas yield at the expense of PyOil.

The C, H, and O balances for each experiment are summarized in **Tables S10-S12**. For the catalytic pyrolysis of pure LDPE, near-complete closure of the C and H balances was achieved across all catalysts, with a slight overestimation in carbon (~2 wt.%) relative to the theoretical input. This minor discrepancy is likely attributed to experimental uncertainties. In contrast, the carbon and oxygen balances for PET and PET–LDPE co-pyrolysis did not close fully, as anticipated. The shortfall is primarily attributed to char formation during PET decomposition, which retains a significant fraction of the C and O content. Additionally, minor coke deposition on the catalyst surface may have further contributed to the observed mass deficits.

With HZSM-5 as the catalyst, an increase in PET content led to a decline in gas yield, primarily due to the higher solid residue produced. For example, pure LDPE pyrolysis yielded only PyOil and PyGas with no detectable solid residue. In contrast, pyrolysis of PET alone resulted in a significant solid residue of 16.8±1 wt.% [49], which contributed to the reduction in oil and gas yields. Additionally, the decreased PyGas yield with higher PET content in the LDPE feed can be attributed to the lower selectivity of HZSM-5 for aromatic compounds. While HZSM-5 exhibits strong cracking activity for LDPE pyrolysis vapors with minimal secondary reactions—yielding an 81.2±0.4 wt.% selectivity for light olefins and a total gas yield of 85.6±0.2 wt.%—PET pyrolysis produces benzoic acid. This acid undergoes decarboxylation and decarbonylation reactions over the HZSM-5 catalyst, forming BTX and benzene derivatives, which contribute to the oil fraction and reduce gas yield. Consequently, an increase in PET content increases the PyOil yields and decreases the PyGas yields.

In comparison, Ga- and Zn-impregnated HZSM-5 catalysts introduce Lewis acid sites that enhance aromatization reactions [75], promoting the conversion of short chain olefins to aromatics, consequently increasing the PyOil yields [30]. During LDPE pyrolysis, Ga- and Zn-modified catalysts yielded significantly lower PyGas amounts (48.3±1.2 wt.% and 43.4±1.6 wt.%, respectively) relative to unmodified HZSM-5 while markedly increasing PyOil yields (51.7±1.2 wt.% and 56.6±1.7 wt.%, respectively). The variation in PyGas and PyOil yields with increased PET content in the LDPE feed was less pronounced when using these modified catalysts. Catalytic upgrading of PET-LDPE co-pyrolysis vapors over Ga-HZSM-5 and Zn-HZSM-5 consistently yielded PyOil in the range of 40-50 wt.%. This reduction in PyOil yield compared to pure LDPE pyrolysis is inevitable due to the inherent production of char and CO/CO_2 gases during PET pyrolysis.

Coke formation is critical for evaluating catalyst performance, particularly in aromatization reactions where coke generation is often unavoidable. However, the micro-pyrolyzer setup used in this study is limited to plastic loadings of 0.4 mg, making the total coke deposition on 20 mg of catalyst too low to be reliably quantified. A meaningful assessment of coke formation requires a larger-scale continuous flow setup with extended time-on-stream (TOS) operation. We plan to address this limitation in future work using our continuous flow reactor, where coke deposition can be measured under more industrially relevant conditions [76].

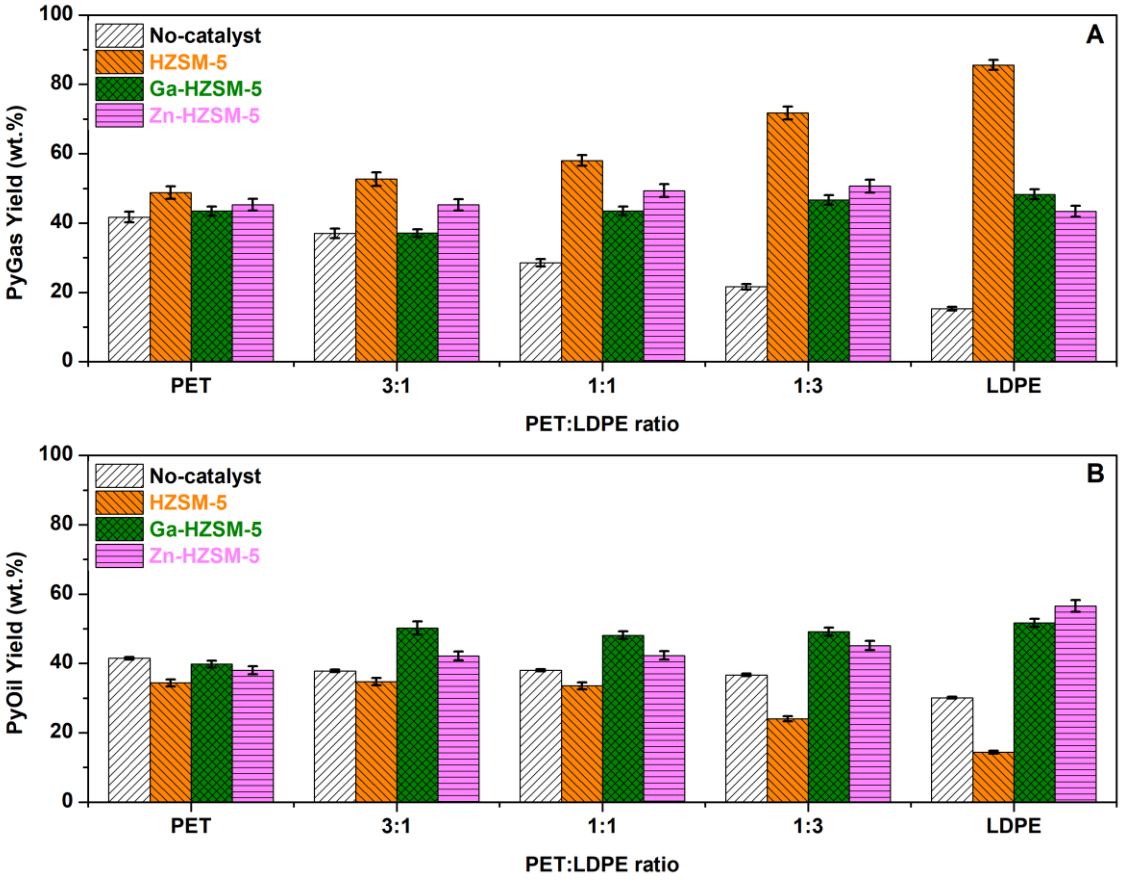

Figure 9. Influence of PET:LDPE ratio and catalyst modification on PyGas (A) and PyOil (B) yields (wt.%) during catalytic cracking of PET and LDPE co-pyrolysis vapors at 600 °C.

The effect of varying PET content in the LDPE feed on product yields was investigated for all three catalysts. To ensure consistency with literature practices [40, 41, 45, 46, 77], product

649 selectivities are reported separately for the PyOil and PyGas fractions, as shown in **Figure 10**.
650 Compared to thermal pyrolysis, the BTX selectivity in the PyOil fraction increased dramatically
651 for all catalysts. This improvement is primarily due to the presence of oxygenates and C_{11+}
652 aliphatics in the PyOil from thermal pyrolysis, which dilute the BTX fraction. In contrast, the
653 catalysts demonstrated excellent deoxygenation, cracking, and aromatization performance,
654 effectively eliminating oxygenates and C_{11+} aliphatics from the PyOil. As a result, the BTX
655 selectivity in PyOil increased from 14.8±1.5 wt.% (the highest BTX selectivity observed in
656 PyOil from thermal pyrolysis with PET) to ≥80 wt.% with catalytic upgrading.

657 For HZSM-5, increasing PET content in the feed led to reduced light olefin selectivity in the
658 gas fraction and a decrease in total PyGas yield. As expected, the drop in light olefin selectivity
659 was proportional to the PET content. However, the trend for PyGas yield was different; as PET
660 content increased, CO and CO_2 production partially compensated for the reduced C_2-C_4 olefin
661 yields, resulting in a less steep decline in total gas yield beyond a 1:1 PET to LDPE ratio.
662 Despite this, the quality of PyGas significantly deteriorated when PET exceeded 50 wt.% of the
663 feed. For instance, light olefins accounted for 95.4±0.4 wt.% of PyGas in pure LDPE pyrolysis.
664 With a 1:3 PET to LDPE ratio, light olefin selectivity dropped to 81.8±0.4 wt.%, and further
665 increased PET content (50 wt.%) caused selectivity to fall to 64.4±0.3 wt.%. Beyond this point,
666 light olefin selectivity fell below 42 wt.%, and CO and CO_2 became predominant in the PyGas.
667 Correspondingly, PyGas yields sharply declined from 85.6±0.2 wt.% to below 50 wt.%.

668 Conversely, PyOil yields increased as the PET to LDPE ratio approached 1:1, with minimal
669 changes beyond that ratio. This increase in PyOil did not substantially affect BTX selectivity,
670 which remained stable between 81–84 wt.%. The co-pyrolysis at 1:3 PET to LDPE ratio
671 achieved the highest BTX selectivity in PyOil at 84.6±2.1 wt.%. Introducing PET to the LDPE
672 feed also promoted polycyclic aromatic hydrocarbon (PAH) formation and decreased the yield

of benzene derivatives in PyOil. Given that the maximum PyOil yield for LDPE-PET co-pyrolysis using HZSM-5 was 34.7±1.2 wt.%—alongside a low-quality PyGas yield of 52.7±2.0 wt.%—HZSM-5 is not an ideal catalyst for BTX production from LDPE-PET mixtures. However, it demonstrated high selectivity for light olefins during LDPE pyrolysis, maintaining high PyGas yields (above 70 wt.%) with a 1:3 PET to LDPE feed ratio. This suggests that HZSM-5 is better suited for targeting gaseous products rather than PyOil in short residence-time systems.

Ga-HZSM-5 followed a similar trend to HZSM-5, with C_2-C_4 olefin selectivity declining as PET content increased. In pure LDPE pyrolysis, light olefin selectivity was 87.1±2.4 wt.% with a total PyGas yield of 48.3±1.2 wt.%, lower than that observed with parent HZSM-5. This decrease is attributed to the role of dispersed GaO_x species (Ga^{3+}, Ga-O-Al) on Ga-HZSM-5 to promote the conversion of light olefins into BTX, benzene derivatives, and PAHs through aromatization. As PET content in the feed increased to 50 wt.%, light olefin selectivity dropped sharply to 51.7±1.4 wt.%. The lowest PyGas yield (37.1±1.4 wt.%) and the highest PyOil yield (50.2±1.8 wt.%) were observed at a 3:1 PET to LDPE ratio. Across all co-pyrolysis experiments, PyOil yields varied slightly (48–50 wt.%), and adding PET to the LDPE feed did not significantly reduced the PyOil yield. However, BTX selectivity changes were more significant; during pure LDPE pyrolysis, BTX selectivity was 89.0±2.2 wt.% in PyOil but dropped to 80.7±2.0 wt.% when PET was introduced.

For Zn-HZSM-5, the decline in light olefin selectivity with increasing PET content was less pronounced compared to HZSM-5 and Ga-HZSM-5. Although light olefin selectivity decreased as PET content rose, the reduction was moderate for Zn-HZSM-5, especially between 1:3 and 1:1 PET to LDPE ratio. For instance, light olefin selectivity in PyGas decreased from 81.8±0.4 wt.% to 64.4±0.3 wt.% with HZSM-5 and from 74.2±2.1 wt.% to 51.8±1.4 wt.% with Ga-

HZSM-5 but only from 69.3±1.9 wt.% to 58.9±1.6 wt.% with Zn-HZSM-5. Similarly, PyGas yield exhibited a minimal decline of ~1 wt.% at these PET levels, compared to decreases of ~13 wt.% and ~3 wt.% for HZSM-5 and Ga-HZSM-5, respectively. These results suggest that Zn-HZSM-5 retains higher yields of light olefins and PyGas, indicating that the aromatization of LDPE-derived olefins (the primary source of light olefins) was less extensive compared to Ga-HZSM-5. This shows the critical influence of the nature of the active sites. Both Zn Ga-based Lewis acid sites are capable of catalyzing deoxygenation (i.e., decarboxylation and decarbonylation) as well as aromatization reactions, albeit with likely differing affinities. For example, in the catalytic pyrolysis of pure LDPE, the Zn-modified catalyst produced a higher BTX yield (50.3±1.3 wt.% based on LDPE feed) and a lower light olefin yield (39.7±1.1 wt.%) compared to Ga-HZSM-5 (44.5±1.1 wt.% BTX and 43.7±1.2 wt.% light olefins). However, under LDPE/PET co-pyrolysis conditions, Ga-HZSM-5 yielded fewer light olefins and a higher overall aromatic yield than Zn-HZSM-5, suggesting more efficient conversion of LDPE-derived olefins into aromatics. This could be attributed to competition between PET-derived oxygenates and LDPE-derived olefins for the same active sites, which may inhibit aromatization on Zn-HZSM-5. In contrast, Ga–O–Al sites likely exhibit a stronger preference for olefin aromatization.

XPS analysis also suggested that a prominent portion of ZnO_x species might be located within the micropores, where pore confinement imposes mass transfer limitations that can reduce the rate of aromatization and subsequent PAH formation. In contrast, Ga species are mainly positioned on the external surface or at pore mouths, providing more accessible sites for LDPE-derived olefins and diolefins to undergo cyclization and condensation, which promotes both aromatics and PAH formation. As a result, while Ga-HZSM-5 produces higher overall aromatics, it also shows a sharper decline in light olefins and greater PAH formation. The possible micropore confinement in Zn-HZSM-5 not only suppresses PAH formation but also

allows it to maintain consistently high BTX selectivity in PyOil (83–87 wt.%) across varying PET-to-LDPE ratios, even as PyOil yields change. Unlike Ga-HZSM-5, the introduction of PET into the LDPE feed had little effect on BTX selectivity with Zn-HZSM-5.

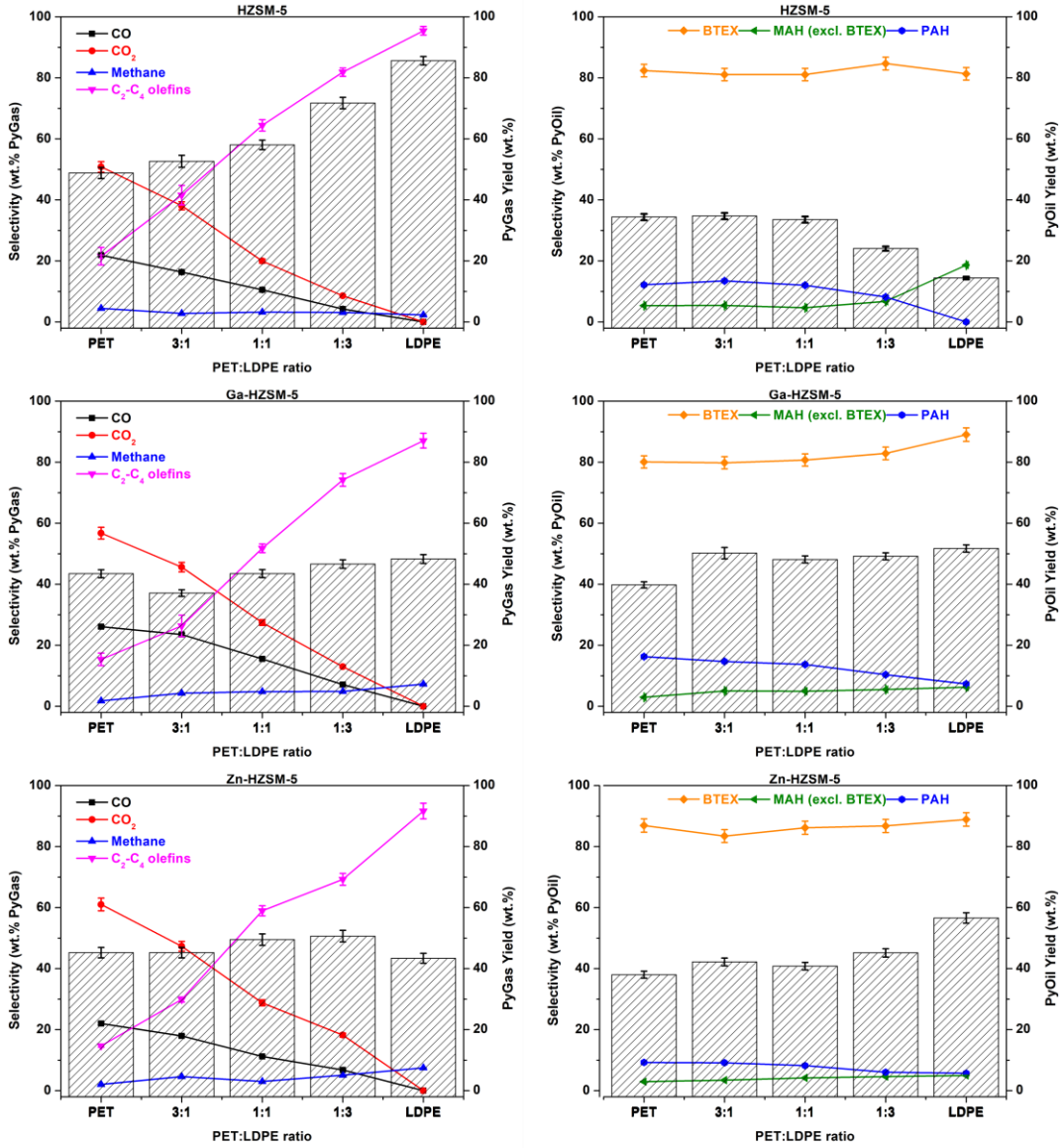

Figure 10. Effect of PET content (wt.%) in the LDPE feed on product selectivity (lines) and PyGas/PyOil yields (bars) during pyrolysis vapor cracking over (Top) HZSM-5, (Middle) Ga-HZSM-5, and (Bottom) Zn-HZSM-5.

The synergistic effects of PET and LDPE co-pyrolysis vapor cracking over parent HZSM-5, Ga-HZSM-5, and Zn-HZSM-5 were investigated, as illustrated in **Figure 11**. The overall magnitude of these synergistic effects on product distribution was less pronounced than thermal pyrolysis. The highest synergy was observed in polyaromatic formation over parent HZSM-5, reaching a maximum of 100%, indicating that PAH formation during co-pyrolysis was twice the combined yield from the individual pyrolysis of PET and LDPE. Notably, none of the catalysts produced C_5-C_{31} aliphatic or oxygenated compounds, making it impossible to evaluate synergistic effects on these products.

The synergy observed for CO production was comparable to that in non-catalytic pyrolysis. Both parent and Ga-HZSM-5 exhibited similar trends when PET to LDPE ratios were varied. Increasing the LDPE content from 3:1 to 1:1 in the PET-LDPE mixture enhanced the positive effect, but further increases did not result in significant changes. Zn-modified HZSM-5 exhibited distinct behavior, showing a more pronounced increase in CO synergy with higher LDPE content. The most notable increase in positive synergy (from 11% to 39%) occurred when the PET to LDPE ratio was shifted from 1:1 to 1:3, indicating that the catalysts promote decarbonylation reactions, with LDPE presence further enhancing this effect.

The synergy for CO_2 production differed from that observed in non-catalytic co-pyrolysis. Although all catalysts increased CO_2 generation in pure PET pyrolysis, co-pyrolysis with LDPE resulted in negative synergy for both the parent and Ga-modified HZSM-5. For the parent HZSM-5, a positive synergy of 8% was noted at a 3:1 PET to LDPE ratio, which turned negative (-6%) when the ratio was adjusted to 1:1, further decreasing to -1% with higher LDPE content. Ga-HZSM-5 showed negative synergy across all ratios, with the magnitude decreasing from -8% at 3:1 to -2% at 1:3. Zn-HZSM-5 exhibited negligible synergy (~3%) at 3:1 and 1:1 PET to LDPE ratios but increased to 33% at a 1:3 ratio.

Parent HZSM-5 showed the highest positive synergies for BTX (40%) and PAH production (89%) at a 1:1 PET to LDPE ratio. In contrast, Ga-modified HZSM-5 displayed the highest BTX synergy (14%) at a 3:1 PET to LDPE ratio, with further LDPE increases eliminating positive BTX synergy. The highest synergy for PAH formation with Ga-HZSM-5 was also observed at the 1:1 ratio, though it was limited to 30%. Zn-HZSM-5 consistently exhibited negative synergy for BTX production across all ratios, with only a positive PAH synergy noted at 3:1 PET to LDPE ratio, which turned negative as LDPE content increased. However, Zn-HZSM-5 showed positive synergy for light olefin formation, suggesting that co-pyrolysis impedes aromatization and instead favors cracking reactions. This indicates that the primary source of aromatic formation with Zn-HZSM-5 stems from PET decarboxylation and decarbonylation, with reduced olefin isomerization and aromatization. This could be due to dehydrogenation and decarboxylation reactions potentially occurring on the same active sites of the catalyst. The decarboxylation of PET-derived products may occupy these active sites, preventing short olefins from binding and undergoing further reactions. This competitive site occupancy limits the isomerization and subsequent aromatization of light olefins, thereby altering the overall product distribution. In contrast, Ga-HZSM-5 demonstrated that the main source of aromatics likely originated from LDPE aromatization. This is evidenced by the negative synergies for CO_2 and light olefins and positive synergies for aromatics, suggesting that light olefins produced from LDPE pyrolysis were more readily converted into aromatics with Ga-HZSM-5 than with Zn-HZSM-5. Furthermore, Ga-HZSM-5 showed the highest synergies for benzene derivatives besides BTX, highlighting its superior alkylation activity among the tested catalysts.

Parent HZSM-5, known for its high C_2-C_4 olefin selectivity, also experienced negative synergy for light olefin production during PET-LDPE co-pyrolysis, similar to Ga-HZSM-5. The negative influence increased with higher PET content, as tripling the PET concentration from

1:3 to 3:1 increased the negative influence from -7.5% to -22.4%. This trend, coupled with the positive synergy for aromatic formation, suggests that co-pyrolysis of PET with LDPE promotes the conversion of light olefins to aromatics over HZSM-5.

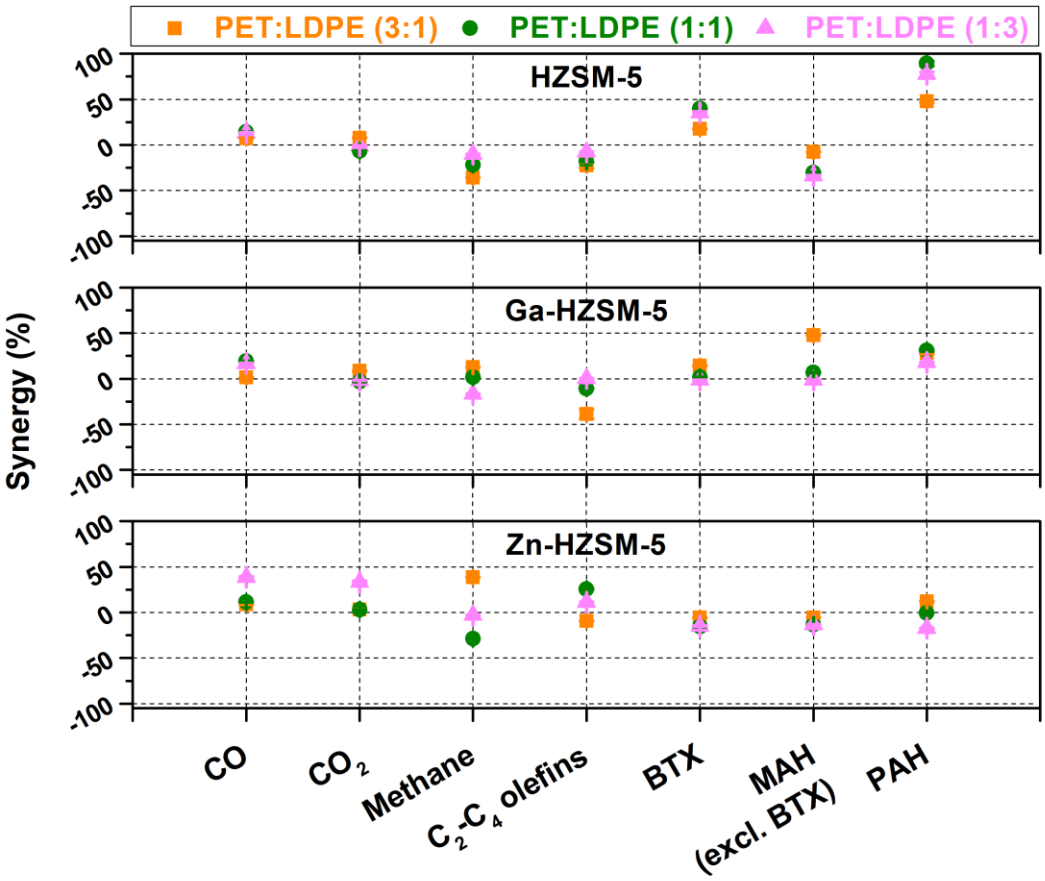

Figure 11. Effect of PET:LDPE ratio on synergy for catalytic upgrading of co-pyrolysis of PET and LDPE over HZSM-5, Ga-HZSM-5, and Zn-HZSM-5 at 600 °C.

4 Conclusion

This study shows that catalytic co-pyrolysis of PET and LDPE using Ga- and Zn-modified HZSM-5 catalysts in a two-stage reactor system offers a promising method for converting mixed plastic waste into valuable products. At a pyrolysis temperature of 600 °C, PET produced

significant amounts of CO_2 (20.0±2.4 wt.%), CO (6.6±0.1 wt.%), and benzoic acid (22.7±0.9 wt.%), along with other oxygenated compounds that degrade the quality of PyOil. The catalytic upgrading with Ga- and Zn-modified HZSM-5 enabled efficient decarboxylation and decarbonylation, improving BTX selectivity and reducing unwanted oxygenated byproducts.

While the parent HZSM-5 catalyst excels at producing light olefins from polyolefins, it showed limited effectiveness with PET-rich feeds, resulting in a lower PyOil yield (34.7±1.3 wt.%) than the modified catalysts. In contrast, Ga- and Zn-promoted HZSM-5 catalysts achieved higher PyOil yields (~50 wt.%) and excellent BTX selectivity (80-89%) during PET and PET-LDPE co-pyrolysis, demonstrating a strong preference for aromatic production across different PET to LDPE ratios. Zn-HZSM-5, in particular, displayed superior BTX selectivity with increasing PET content, underscoring its robustness in processing diverse mixed plastic waste streams.

The versatility of Ga- and Zn-impregnated HZSM-5 for producing BTX-rich PyOil makes these catalysts highly suitable for mixed waste streams containing both PET and polyolefins. These modified catalysts not only improve selectivity toward valuable aromatics but also maintain high PyOil yields with substantial BTX content (80-89%) across a range of PET:LDPE ratios. This catalytic system is well-suited for recycling scenarios where precise waste sorting is difficult, providing a sustainable pathway for plastic waste valorization. The process yields products suitable for chemical and fuel applications, reducing dependence on petroleum-based resources and supporting the transition to a circular economy.

5 Acknowledgment

We gratefully acknowledge the financial support of the Flemish Government and Flanders Innovation & Entrepreneurship (VLAIO) through the Moonshot project PREFER (HBC.2020.2609) and Catalisti clusterSBO project WATCH (HBC.2019.0001). The research leading to these results has also received funding from the European Research Council (ERC)

under the European Union's Horizon 2020 research and innovation programme / ERC grant agreement n° 818607 and European Union's Horizon Europe ERC Advanced Grant e-CRACKER (ERC-2023-ADG) under grant agreement N° 101142065.

References

1. Dogu, O., et al., *The chemistry of chemical recycling of solid plastic waste via pyrolysis and gasification: State-of-the-art, challenges, and future directions.* Progress in Energy and Combustion Science, 2021. **84**.
2. Khatun, R., et al., *Bibliometric analysis of research trends on the thermochemical conversion of plastics during 1990–2020.* Journal of Cleaner Production, 2021. **317**: p. 128373.
3. Akin, O., et al., *Chemical recycling of plastic waste to monomers: Effect of catalyst contact time, acidity and pore size on olefin recovery in ex-situ catalytic pyrolysis of polyolefin waste.* Journal of Analytical and Applied Pyrolysis, 2023. **172**.
4. Eschenbacher, A., et al., *Maximizing light olefins and aromatics as high value base chemicals via single step catalytic conversion of plastic waste.* Chemical Engineering Journal, 2022. **428**: p. 132087.
5. Akin, O., et al., *Tailored HZSM-5 catalyst modification via phosphorus impregnation and mesopore introduction for selective catalytic conversion of polypropylene into light olefins.* Journal of Analytical and Applied Pyrolysis, 2024. **181**.
6. Eschenbacher, A., et al., *Boron-Modified Mesoporous ZSM-5 for the Conversion of Pyrolysis Vapors from LDPE and Mixed Polyolefins: Maximizing the C-2-C-4 Olefin Yield with Minimal Carbon Footprint.* Acs Sustainable Chemistry & Engineering, 2021. **9**(43): p. 14618-14630.
7. Goshayeshi, B., et al., *Selective catalytic conversion of model olefin and diolefin compounds of waste plastic pyrolysis oil: Insights for light olefin production and coke minimization.* Chemical Engineering Journal, 2024. **500**.
8. Eschenbacher, A., et al., *Highly selective conversion of mixed polyolefins to valuable base chemicals using phosphorus-modified and steam-treated mesoporous HZSM-5 zeolite with minimal carbon footprint.* Applied Catalysis B-Environmental, 2022. **309**.
9. *The Circular Economy for Plastics – A European Overview*, in *Plastics Europe Circularity Report*, P. Europe, Editor. 2022, Plastics Europe AISBL: Belgium.
10. Ragaert, K., L. Delva, and K. Van Geem, *Mechanical and chemical recycling of solid plastic waste.* Waste Management, 2017. **69**: p. 24-58.
11. Horodytska, O., F.J. Valdés, and A. Fullana, *Plastic flexible films waste management - A state of art review.* Waste Management, 2018. **77**: p. 413-425.
12. Sivagami, K., et al., *Catalytic pyrolysis of polyolefin and multilayer packaging based waste plastics: A pilot scale study.* Process Safety and Environmental Protection, 2021. **149**: p. 497-506.
13. Okonsky, S.T., J.V.J. Krishna, and H.E. Toraman, *Catalytic co-pyrolysis of LDPE and PET with HZSM-5, H-beta, and HY: experiments and kinetic modelling.* Reaction Chemistry & Engineering, 2022. **7**(10): p. 2175-2191.
14. Du, S.C., et al., *Conversion of Polyethylene Terephthalate Based Waste Carpet to Benzene-Rich Oils through Thermal, Catalytic, and Catalytic Steam Pyrolysis.* Acs Sustainable Chemistry & Engineering, 2016. **4**(5): p. 2852-2860.

15. Bhanderi, K.K., J.R. Joshi, and J.V. Patel, *Recycling of polyethylene terephthalate (PET Or PETE) plastics - An alternative to obtain value added products: A review.* Journal of the Indian Chemical Society, 2023. **100**(1).
16. Kumagai, S., et al., *Catalytic Pyrolysis of Poly(ethylene terephthalate) in the Presence of Metal Oxides for Aromatic Hydrocarbon Recovery Using Tandem μ-Reactor-GC/MS.* Energy & Fuels, 2020. **34**(2): p. 2492-2500.
17. Konarova, M., et al., *Integrating PET chemical recycling with pyrolysis of mixed plastic waste via pressureless alkaline depolymerization in a hydrocarbon solvent.* Waste Management, 2024. **174**: p. 24-30.
18. Artetxe, M., et al., *Operating Conditions for the Pyrolysis of Poly-(ethylene terephthalate) in a Conical Spouted-Bed Reactor.* Industrial & Engineering Chemistry Research, 2010. **49**(5): p. 2064-2069.
19. Yoshioka, T., et al., *High selective conversion of poly(ethylene terephthalate) into oil using Ca(OH).* Chemistry Letters, 2004. **33**(3): p. 282-283.
20. Grause, G., et al., *Effect of temperature management on the hydrolytic degradation of PET in a calcium oxide filled tube reactor.* Chemical Engineering Journal, 2011. **166**(2): p. 523-528.
21. Kumagai, S., et al., *Catalytic Degradation of Poly(ethylene terephthalate) for Benzene-rich Oil Recovery Using Metal Hydroxides.* Chemistry Letters, 2014. **43**(5): p. 637-639.
22. Kumagai, S., et al., *Tandem μ-reactor-GC/MS for online monitoring of aromatic hydrocarbon production*

CaO-catalysed PET pyrolysis. Reaction Chemistry & Engineering, 2017. **2**(5): p. 776-784.
23. Rahman, M.M., R.H. Liu, and J.M. Cai, *Catalytic fast pyrolysis of biomass over zeolites for high quality bio-oil - A review.* Fuel Processing Technology, 2018. **180**: p. 32-46.
24. Carlson, T.R., et al., *Catalytic fast pyrolysis of glucose with HZSM-5: The combined homogeneous and heterogeneous reactions.* Journal of Catalysis, 2010. **270**(1): p. 110-124.
25. Du, S.C., et al., *Coke formation of model compounds relevant to pyrolysis bio-oil over ZSM-5.* Applied Catalysis a-General, 2016. **513**: p. 67-81.
26. Kumagai, S., et al., *Decomposition of Gaseous Terephthalic Acid in the Presence of CaO.* Industrial & Engineering Chemistry Research, 2011. **50**(4): p. 1831-1836.
27. Liu, X.L., et al., *Catalytic Pyrolysis of Nonedible Oils for the Production of Renewable Aromatics Using Metal-Modified HZSM-5 Catalysts.* Acs Omega, 2022. **7**(22): p. 18953-18968.
28. Qian, K.Z., et al., *Aromatic production from high-density polyethylene over zinc promoted HZSM-5.* Applied Catalysis B-Environmental, 2023. **339**.
29. Liu, P.Y., et al., *Suitable location of Lewis acid over ZnOH+/HZSM-5 catalysts effectively enhance dehydrogenation activity and catalyze the aromatization process of C6 olefins in MTA.* Fuel, 2024. **357**.
30. Fu, L.C., et al., *Catalytic Pyrolysis of Waste Polyethylene Using Combined CaO and Ga/ZSM-5 Catalysts for High Value-Added Aromatics Production.* Acs Sustainable Chemistry & Engineering, 2022. **10**(29): p. 9612-9623.
31. Barzallo, D., et al., *Bifunctional Catalytic Performance of Zn/ZSM-5 in the Aromatization of LPG and the Conversion of Pyrolytic Gases from Recycled Polypropylene.* ChemEngineering, 2024. **8**(6): p. 108.
32. Bhan, A. and W. Nicholas Delgass, *Propane Aromatization over HZSM-5 and Ga/HZSM-5 Catalysts.* Catalysis Reviews, 2008. **50**(1): p. 19-151.

33. Wang, Y.Z., et al., *Catalytic Pyrolysis of Polyethylene for the Selective Production of Monocyclic Aromatics over the Zinc-Loaded ZSM-5 Catalyst.* Acs Omega, 2022. **7**(3): p. 2752-2765.
34. Tamiyakul, S., S. Anutamjarikun, and S. Jongpatiwut, *The effect of Ga and Zn over HZSM-5 on the transformation of palm fatty acid distillate (PFAD) to aromatics.* Catalysis Communications, 2016. **74**: p. 49-54.
35. Uslamin, E.A., et al., *Gallium-promoted HZSM-5 zeolites as efficient catalysts for the aromatization of biomass-derived furans.* Chemical Engineering Science, 2019. **198**: p. 305-316.
36. Biriaei, R., S. Madadi, and S. Kaliaguine, *Mesostructured Zn/ZSM-5 Zeolite as Catalyst for Furan Deoxygenation.* Chemistryselect, 2022. **7**(4).
37. Moogi, S., et al., *Enhancement of bioaromatics production from food waste through catalytic pyrolysis over Zn and Mo-loaded HZSM-5 under an environment of decomposed methane.* Chemical Engineering Journal, 2022. **446**.
38. Lai, P.C., et al., *Methanol aromatization over Ga-doped desilicated HZSM-5.* Rsc Advances, 2016. **6**(71): p. 67361-67371.
39. Muringayil Joseph, T., et al., *Polyethylene terephthalate (PET) recycling: A review.* Case Studies in Chemical and Environmental Engineering, 2024. **9**: p. 100673.
40. Jia, H., et al., *Catalytic Fast Pyrolysis of Poly (Ethylene Terephthalate) (PET) with Zeolite and Nickel Chloride.* Polymers, 2020. **12**(3).
41. Tuly, S.S., M.M.S. Joarder, and M.E. Haque, *Liquid Fuel Production by Pyrolysis of Polythene and PET Plastic.* 8th Bsme International Conference on Thermal Engineering, 2019. **2121**.
42. Osman, A.I., et al., *Pyrolysis kinetic modelling of abundant plastic waste (PET) and in-situ emission monitoring.* Environmental Sciences Europe, 2020. **32**(1).
43. Abbas-Abadi, M.S., et al., *Challenges and opportunities of light olefin production via thermal and catalytic pyrolysis of end-of-life polyolefins: Towards full recyclability.* Progress in Energy and Combustion Science, 2023. **96**.
44. Okonsky, S.T., N.R. Hogan, and H.E. Toraman, *Effect of pyrolysis operating conditions on the catalytic co-pyrolysis of low-density polyethylene and polyethylene terephthalate with zeolite catalysts.* Aiche Journal, 2024.
45. Park, C., et al., *Pyrolysis of Polyethylene Terephthalate over Carbon-Supported Pd Catalyst.* Catalysts, 2020. **10**(5).
46. Gulab, H., S. Malik, and K. Hussain, *Catalytic Pyrolysis of Polyethylene Terephthalate and Its Copyrolysis with Polyethylene.* Environmental Engineering Science, 2024. **41**(8): p. 327-336.
47. Olam, M. and H. Karaca, *Characterization of products obtained of waste polyethylene terephthalate by pyrolysis.* Environmental Progress & Sustainable Energy, 2022. **41**(4).
48. Jiang, M.K., et al., *Chemical catalytic upgrading of polyethylene terephthalate plastic waste into value-added materials, fuels and chemicals.* Science of the Total Environment, 2024. **912**.
49. Locaspi, A., et al., *A lumped kinetic model and experimental investigation of poly(ethylene terephthalate) condensed-phase pyrolysis.* Chemical Engineering Journal, 2024: p. 156955.
50. Iisa, K., et al., *Ga/ZSM-5 catalyst improves hydrocarbon yields and increases alkene selectivity during catalytic fast pyrolysis of biomass with co-fed hydrogen.* Green Chemistry, 2020. **22**(8): p. 2403-2418.

51. He, Q., et al., *Enhancing catalytic pyrolysis of polypropylene using mesopore-modified HZSM-5 catalysts: insights and strategies for improved performance.* Frontiers in Chemical Engineering, 2024. **6**.
52. Deutschmann, O. and L.D. Schmidt, *Modeling the partial oxidation of methane in a short-contact-time reactor.* Aiche Journal, 1998. **44**(11): p. 2465-2477.
53. de St Laumer, J.Y., et al., *Prediction of response factors for gas chromatography with flame ionization detection: Algorithm improvement, extension to silylated compounds, and application to the quantification of metabolites.* Journal of Separation Science, 2015. **38**(18): p. 3209-3217.
54. Gim, M.Y., et al., *Coaromatization of methane and propane over Ga supported on HZSM-5 catalysts: The effect of mesoporosity on deactivation behavior.* Fuel, 2021. **304**.
55. Alotibi, M.F., et al., *ZSM-5 Zeolite Based Additive in FCC Process: A Review on Modifications for Improving Propylene Production.* Catalysis Surveys from Asia, 2020. **24**(1): p. 1-10.
56. Seemann, T., et al., *Argon physisorption for pore analysis of mudrocks, clays, and engineered analogues: is argon a better choice than nitrogen and carbon dioxide?* Clays and Clay Minerals, 2025. **73**: p. e2.
57. Swiqtkowski, A., *Surface Area and Porosity Determinations by Physisorption. Measurement, Classical Theories and Quantum Theory.* Przemysl Chemiczny, 2020. **99**(5): p. 670-671.
58. Katada, N., et al., *Determination of the acidic properties of zeolite by theoretical analysis of temperature-programmed desorption of ammonia based on adsorption equilibrium.* Journal of Physical Chemistry B, 1997. **101**(31): p. 5969-5977.
59. Jin, R.Z., et al., *Effect of CO2 on the catalytic performance of Zn/ZSM-5 towards the conversion of methanol to aromatics.* Fuel, 2023. **332**.
60. Gao, J., et al., *Evolution of Zn Species on Zn/HZSM-5 Catalyst under H*

Pretreated and its Effect on Ethylene Aromatization. Chemcatchem, 2019. **11**(16): p. 3892-3902.
61. Niu, X.J., et al., *Influence of preparation method on the performance of Zn-containing HZSM-5 catalysts in methanol-to-aromatics.* Microporous and Mesoporous Materials, 2014. **197**: p. 252-261.
62. Fricke, R., et al., *Incorporation of gallium into zeolites: Syntheses, properties and catalytic application.* Chemical Reviews, 2000. **100**(6): p. 2303-2405.
63. Jia, S., S. Wu, and Z. Meng, *Study on the active center of Ga2O3/HZSM-5 catalyst.* Applied Catalysis A: General, 1993. **103**(2): p. 259-268.
64. Xiao, H., et al., *A highly efficient Ga/ZSM-5 catalyst prepared by formic acid impregnation and*

treatment for propane aromatization. Catalysis Science & Technology, 2015. **5**(8): p. 4081-4090.
65. Nowak, I., et al., *Effect of H-O pre-treatments on the state of gallium in Ga/H-ZSM-5 propane aromatisation catalysts.* Applied Catalysis a-General, 2003. **251**(1): p. 107-120.
66. Jahangiri, H., et al., *Ga/HZSM-5 Catalysed Acetic Acid Ketonisation for Upgrading of Biomass Pyrolysis Vapours.* Catalysts, 2019. **9**(10).
67. Buxbaum, L.H., *The Degradation of Poly(ethylene terephthalate).* Angewandte Chemie International Edition in English, 1968. **7**(3): p. 182-190.

68. Levchik, S.V. and E.D. Weil, *A review on thermal decomposition and combustion of thermoplastic polyesters.* Polymers for Advanced Technologies, 2004. **15**(12): p. 691-700.
69. Yousef, S., et al., *Pyrolysis Kinetic Behavior and Thermodynamic Analysis of PET Nonwoven Fabric.* Materials, 2023. **16**(18).
70. Hujuri, U., A.K. Ghoshal, and S. Gumma, *Temperature-Dependent Pyrolytic Product Evolution Profile for Polyethylene Terephthalate.* Journal of Applied Polymer Science, 2013. **130**(6): p. 3993-4000.
71. Wu, Y.H., et al., *Unraveling the Structure-Activity-Stability Relationship over Gallium-Promoted HZSM-5 Nanocrystalline Aggregates for Propane Aromatization.* Langmuir, 2024. **40**(23): p. 11998-12008.
72. Qian, K.Z., et al., *Aromatization of HDPE and PP over Ga-promoted zeolite: Effects of pretreatment and zeolite type.* Fuel, 2024. **357**.
73. Wongnongwa, Y., et al., *Local structure elucidation and reaction mechanism of light naphtha aromatization over Ga embedded H-ZSM-5 zeolite: Combined DFT and experimental study.* Microporous and Mesoporous Materials, 2020. **306**.
74. Ramos, R., et al., *Enhanced Production of Aromatic Hydrocarbons by Rapeseed Oil Conversion over Ga and Zn Modified ZSM-5 Catalysts.* Industrial & Engineering Chemistry Research, 2016. **55**(50): p. 12723-12732.
75. Espindola, J.S., et al., *Conversion of furan over gallium and zinc promoted ZSM-5: The effect of metal and acid sites.* Fuel Processing Technology, 2020. **201**.
76. Goshayeshi, B., et al., *Enhancing polystyrene recycling: Temperature-responsive of pyrolysis in a pilot-scale vortex reactor.* Journal of Analytical and Applied Pyrolysis, 2025. **187**.
77. Straka, P., O. Bicáková, and M. Supová, *Slow pyrolysis of waste polyethylene terephthalate yielding paraldehyde, ethylene glycol, benzoic acid and clean fuel.* Polymer Degradation and Stability, 2022. **198**.